12-2019

# Exploring Convergence of Snake Skin-Inspired Texture Designs and Additive Manufacturing for Mechanical Traction

Catherine Sue Tiner
*University of Arkansas, Fayetteville*

Exploring Convergence of Snake Skin-Inspired Texture Designs and Additive Manufacturing for Mechanical Traction

A thesis submitted in partial fulfillment
of the requirements for the degree of
Master of Science in Microelectronics-Photonics

by

Catherine Sue Tiner
Oklahoma State University
Bachelor of Science in Mechanical Engineering, 2017

December 2019
University of Arkansas

This thesis is approved for recommendation to the Graduate Council.

| | |
|---|---|
| _____ | _____ |
| Ajay Malshe, Ph.D.<br>Thesis Director | Gregory Salamo, Ph.D.<br>Thesis Director |
| _____ | _____ |
| Arun Nair, Ph.D.<br>Committee Member | Salil Bapat, Ph.D.<br>Committee Member |
| _____ | |
| Rick Wise, Ph.D.<br>Ex-officio Member | |

The following signatories attest that all software used in this thesis was legally licensed for use by Catherine Tiner for research purposes and publication.

| | |
|---|---|
| _____ | _____ |
| Ms. Catherine Tiner | Dr. Ajay Malshe, Thesis Director |

_____

Dr. Gregory Salamo, Thesis Director

This thesis was submitted to http://www.turnitin.com for plagiarism review by the TurnItIn company's software. The signatories have examined the report on this thesis that was returned by TurnItIn and attest that, in their opinion, the items highlighted by the software are incidental to common usage and are not plagiarized material.

| | |
|---|---|
| _____ | _____ |
| Dr. Rick Wise, Program Director | Dr. Ajay Malshe, Thesis Director |

_____

Dr. Gregory Salamo, Thesis Director

## Abstract

This research focuses on the understanding, development, and additive manufacture of a 3D printed snake skin-inspired texture pattern. The design functionalities of snake skin were determined through the study of the snake species *Python Regius* otherwise known as the ball python. Each scale of a snake has hierarchical texture with hexagonal macro-patterns aligned on the ventral surface of the skin with overriding anisotropic micro textured patterns such as denticulations and fibrils. Using a laser-powder bed fusion (L-PBF) process, 420 stainless steel samples were 3D printed which closely resemble the above described directional texture of natural snake skin. This printed surface was tested for the understanding of friction management using a pin-on-disk tribometer in relation to the directional antislippery behavior of the snake. This thesis explores the convergence of a bio-inspired design with additive manufacturing for realization of functional surfaces.

**Acknowledgements**

This thesis represents all of my hard work over my past few years here at the University of Arkansas. First, I would like to thank my advisor, Dr. Ajay Malshe, for supporting me and guiding me along this path of scientific pursuit. In addition, I would also like to thank Dr. Salil Bapat for teaching me the ropes and helping to support my growth as a researcher.

I am grateful to those who have assisted me in carrying out my research, namely Dr. Subrata Deb Nath and Dr. Atre from the University of Louisville, without who the designs would not have come into fruition. I would also like to thank my fellow cohort members in Cohort 20 and other friends that I made along the way. May we continue to laugh together and support each other during hard times. My sincere thanks to Dr. Rick Wise, who suggested I pursue a graduate degree and also to my thesis committee members, Dr. Salamo and Dr. Nair, for their support over the course of this research.

Lastly, I would like to express sincere gratitude to my parents, Paul and Jennifer, for their love and support over the years.

*Financial Support:* I would like to acknowledge partial funding support by the National Science Foundation and the Arkansas EPSCoR Program, ASSET II (Grant Number 1457888) . I would also like to acknowledge partial funding from the 21$^{st}$ professorship funding courtesy of Dr. Malshe.

## Table of Contents

## List of Figures

## List of Tables

**List of Published Papers Used in This Thesis**

Parts of Chapters 2, 3, and 4 were originally published as:

Tiner, C., Bapat, S., Nath, S. D., Atre, S. V., and Malshe, A. (2019). Exploring Convergence of Snake-Skin-Inspired Texture Designs and Additive Manufacturing for Mechanical Traction. Procedia Manufacturing, 34, 640-646. (NAMRC 47 publication).

# Chapter 1

## Introduction

Nature has adapted and continued to evolve in order to combat continuously changing and harsh environmental conditions [1]. Nature provides multiple unique physical designs for different surfaces and interfaces which are crucial for survival and can be applied to the growing population for continued learning about sustainable products and their designs. Over the past few decades, both engineers and scientists have learned from the nature around them for the synthesis of bio-inspired designs for advanced product applications.

Interaction between the biological species and the environment occurs through the outside layers covering the plants or animals, typically known as skin. This skin or surface of a species serves as the primary interface between the species itself and the ground or other contact area(s) made through movement. Since the surface of skin is the outermost layer, it is constantly put against the environmental factors native to their biome and habitat [2]. Some potentially dangerous factors these species can be subjected against include harsh temperatures, rough terrain, the absence of light, potential disease and bacteria, and so on. Due to the many threats a species must combat to continue survival, the species' outside layer of skin itself has to adapt in the form of multi-functional surfaces which are used as a "defense mechanism" for combat while also applying the desired surface design strategies to acquire those functions. Exploring the convergence of such designs for manufacturing processes and mechanical applications is the focus of this research.

In particular, for this research, a focus was put on species that have shown that they are a highly capable of survival in various terrains, snakes. Snakes provide a unique case study in

understanding the biological mechanical functions of surfaces. While they have no legs, arms, or other movement focused appendages, they can still move quickly and efficiently on a variety of terrains, as if they are natures 'soft robots.' It was discovered that snake scales are covered in small u-shaped micro textures [3]. These textures contribute to the snake's ability to move forward with controlled mechanical manipulation of locomotion. This unique function driven by the unique surface design architectures, referred to as a 'texture' from here onwards, could be useful for several industrial engineering applications for friction management and, thus, were of interest for this research [3].

Surface textures are one of the key design tools in nature's tool box to realize multi-functional surfaces [2]. Textures can be further sub-divided into six components as shown in Figure 1. These are the orientation, shape, size, aspect ratio, periodicity, and the hierarchical arrangement of the features. A snake's design is made up of macro and micro features. Both the macro and micro features play an important role in the snakes' locomotion capabilities and each of the previously mentioned aspects affect the design and manufacturing of snake skin texture.

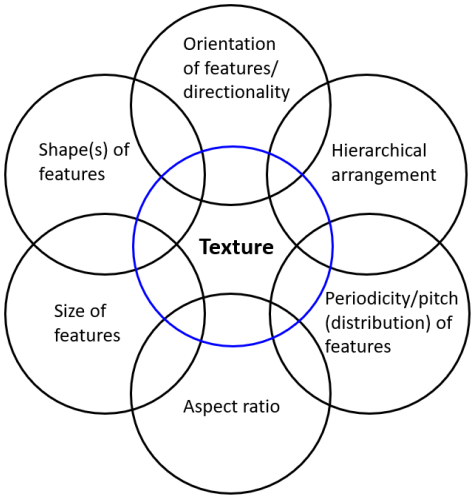


Figure 1. Surface texture components [1].

The main goal for this research was to understand the role of the macro scales and subsequent micro scale surface textures found on snake skin and to manufacture and test snake skin inspired hierarchical texture designs. A laser fusion process was explored as an additive manufacturing (AM) process to synthesize hierarchical textures. Tribological tests were performed on the 3D printed metal texture patterns and surface characterization was accomplished by using a laser scanning microscope. The following chapters discuss the fundamental scientific exploration of the snake skin design, manufacturing of bio-inspired textures, and tribological test results and characterization.

# Chapter 2

## Detailed Review of Snake Scales

To understand the roles of both the macro and micro texture designs found on snake skin, a detailed study of snake skin was first conducted. This chapter discusses the findings and subsequent review.

### 2.1 Snake Scales

Scales cover the entire body of a snake and their design and functionality varies according to their location on the snakes' body. These scales come in a variety of shapes and sizes and, when all are combined together, form snake skin. The scales of a snake have many purposes. Some of these include protection from predators and the environment through color manipulation, moisture retainment and, most importantly, assisting in their locomotion capabilities.

There are three main classes of body scales in snakes [4]. The first, found in all snakes, are the ventral scales. These scales are found on the belly of the snake and extend from the neck to the tail. Ventral scales are typically long and hexagonal in shape. Theses scales are also constantly in contact (or interface) with the environment, e.g. ground, making them the most essential in frictional manipulation during the locomotion of a snake. The other two types of scales are smooth or keeled dorsal scales. These scales are found on the rest of the body of the snake other than the belly. Smooth scales have a smooth surface capable of reflecting light. This manipulation of light gives the snake a glossy appearance. Snakes with smooth scales use this reflective coloring to signal to their predators that they are poisonous. Keeled scales, on the other hand, have a raised slit that runs through the middle of the scale. Unlike smooth scales, the slit

reduces the reflectivity on the scale, which allows for camouflage due to the dull appearance. Many snakes with keeled scales have scales that are also green and brown in color. Due to the combination of the anti-reflective properties and coloring of the scales, snakes with these patterns are venomous and rely on the dullness of their scales to sneak up on prey.

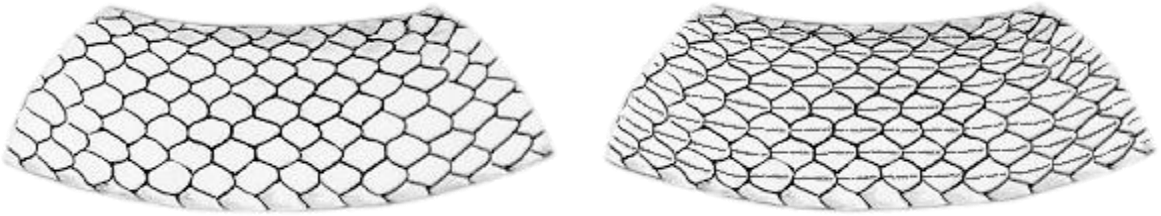

Figure 2. Smooth and keeled dorsal scales [4].

The ventral scales of a snake, since they are constantly against the ground or other surfaces, are the main contributor that effects the frictional properties during movement of a snake. The movement of a snake occurs due to two forces, one due to frictional resistance in the backward direction, and the other due to the propulsion in the forward direction by the muscles of the snake. The hierarchical and directional textures on the snake skin are responsible for the anisotropic friction properties desired for snake movement. Additionally, the coefficient of friction (COF) is managed by natural lubrication a snake produces excreted by these scales, but some also have small hinges or membranes that helps the snake grip onto objects. These membranes are one of the reasons that snakes can grip and climb up tree branches [5].

### 2.2 Anatomy of Snake Skin

Similar to many other reptiles, the skin of a snake has two different layers. These layers are the dermis and epidermis. The dermis is the innermost layer of the skin. This layer contains the tissues, nerves, and other nervous system physiology. On the other hand, the epidermis is the

outermost layer of the skin. This layer contains the cells that produce melanin and melatonin along with some of the other cells that protect the snake from diseases [6, 7, 8, 9].

For the purpose of this research, it was decided to study the epidermal layer of snake skin since the epidermal layer is the outermost layer of the two and therefore colludes closely with the frictional properties of the skin as it rubs against the terrain the snake is traversing upon. Figure 3 depicts the cross section of the two core layers along with the different sublayers that occur in each of the epidermis and dermis main layers.

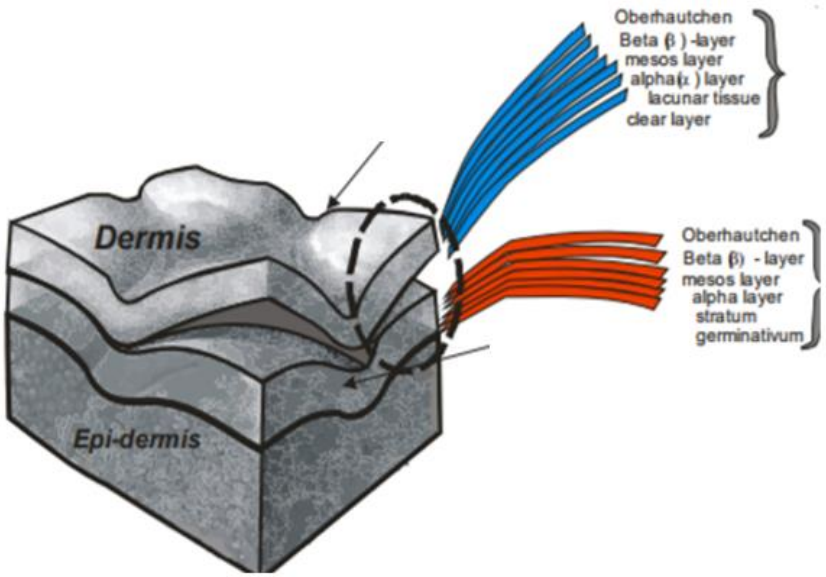


Figure 3. The layers and sublayers of snake skin [6].

As shown by Figure 3, while there are two main layers of skin, the dermis and epidermis, each of those layers possess many different sublayers that each have an important role in the overall system. On the epidermal scales, the epidermis sublayers condense and form a keratinized body that protects the snake from the outside elements. The outermost sublayer of skin is where keratinization occurs. This layer is also the layer that sheds when enough damage occurs on the skin. Beneath that sublayer, more sublayers that allow the snake to stretch are

found. Under the epidermal sublayers, dermal sublayers are present. All of these layers combined create the full snake skin [6, 10].

### 2.3 Hierarchical Textures

As mentioned in Section 2.1 Snake Scales, ventral scales are one of the main classification of scales found on a snake's body and are found along the belly of the snake. These ventral scales are considered the macro structure of the snake. In addition, a feature predominantly found on most ventral scales are hook like features called fibrils. Fibrils are hair-like tendrils that can be found on the surface of the skin of the snake. These fibrils are microscopic in diameter and are a few microns (~1-3 µm) in length. Denticulations, or u-shaped patterns, also occur on the surface of the skin. The combination of these two features are essential in the frictional properties of snake skin during locomotion [3, 11, 12]. A visual summary of the macro and micro textures of snake skin is shown in Figure 4.

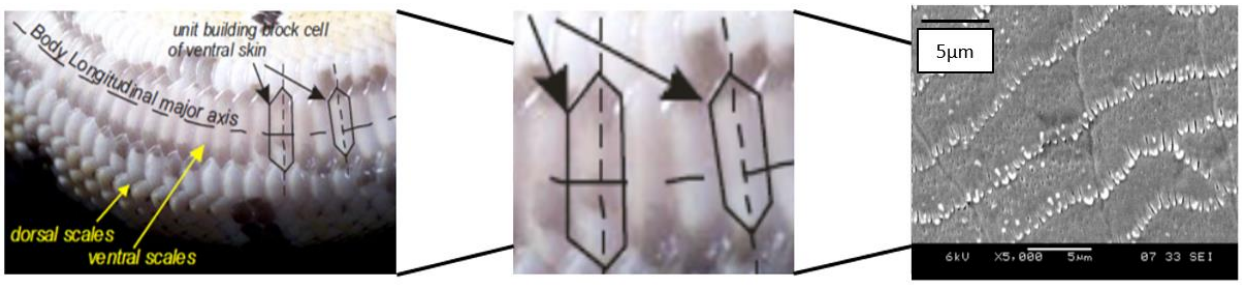


Figure 4. Representation of macro and micro features [11].

The patterning of the fibrils and denticulations vary from snake to snake as each snake species has their own unique arrangement of the features. For some, the fibrils and denticulations are located in a more central area of the skin whereas for others they occur near the outer ridges where ventral scales and dorsal scales meet. The placement of the features has an effect in the locomotional pattern a snake travels in [11, 13].

The three key design properties that determine the friction and wear management in snake skin are orientation, size of the features, and periodicity of the macroscale scales and microscale denticulations. In addition to the texture and design parameters, the positioning of the above discussed features also needs to be considered to accurately understand and model the snake skin for locomotion. As seen in Figure 4, the most predominate feature in the micro pattern is the texture patterning that occurs throughout the macro scale. Each of these textures is u-shaped and rounded. These features manipulate the area of contact with the surfaces, as well as their anisotropic directional orientation, allowing for the act of unidirectional locomotion.

Overall, the features shape, size, distribution, and orientation play a key role in the movement of a snake. Therefore, the texturing of the surface of each hexagonal densely packed scale is vital in determining what anisotropic frictional properties exist in each individual snake skin scale.

### 2.4 Modes of Locomotion

Creatures without limbs, such as snakes, are typically both slender and flexible. Since they cannot take advantage of the bone structure that allows walking or other patterns of movement, these animals adapted to use different forms of locomotion. To overcome these challenges, snakes have learned to propel themselves forwards in various ways. The motion of a snake is a balance between the forces generated by their muscles and the traction generated by friction. This balance created different patterns (modes) of locomotion described below.

There are four main modes of locomotion that a snake travels in. These four patterns are known as serpentine, concertina, crotaline (also known as sidewinding), and rectilinear. The form of travel for each of these patterns can be seen in the Figure 5 below.

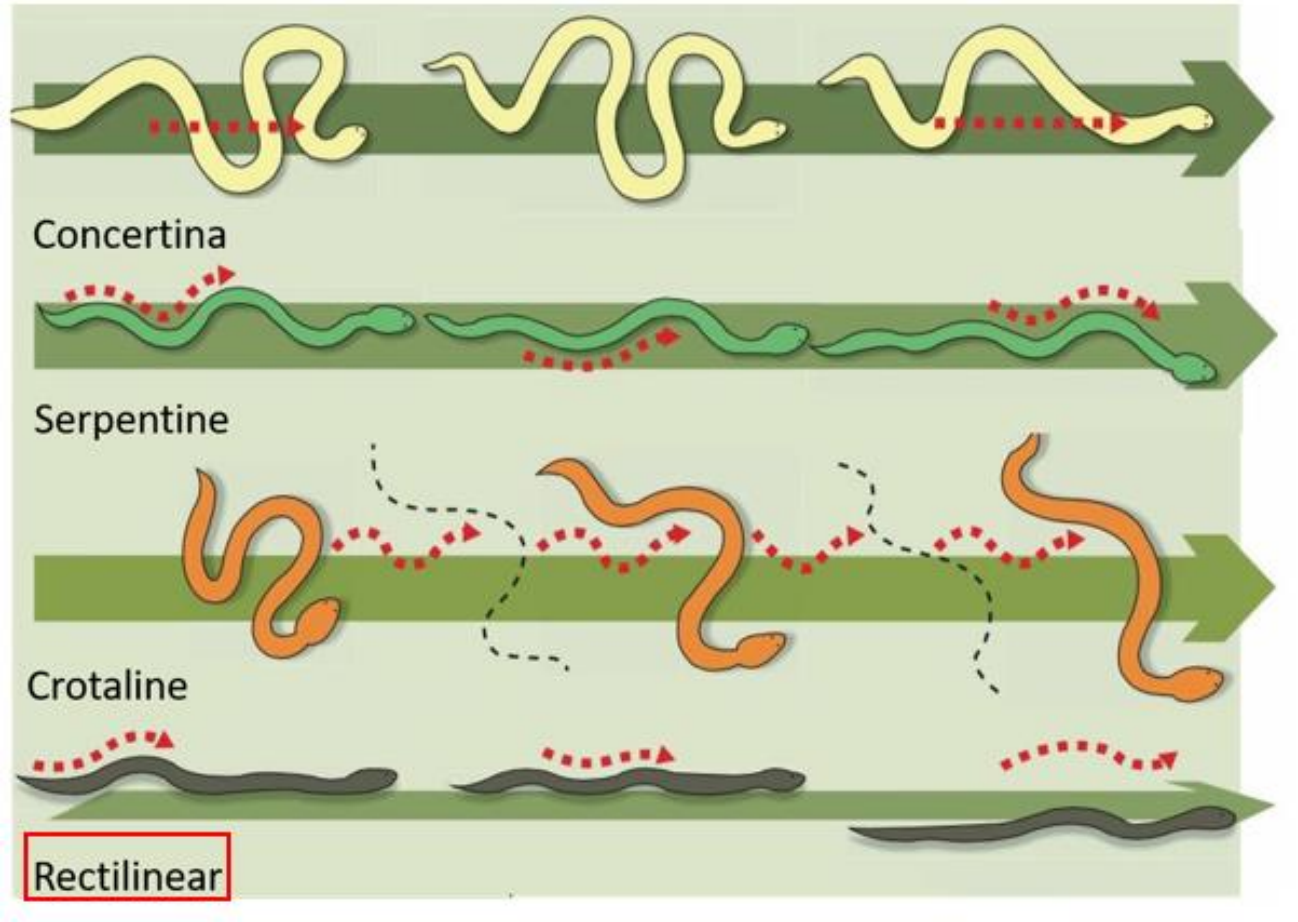


Figure 5. Patterns of snake movement [5].

Concertina locomotion occurs when the frictional resistance, as mentioned in the serpentine movement, is low. This type of movement occurs when the snake needs to move straight in a forward pattern or while in a tight circular space. Since the body is typically always pressed up against a wall or opposing surface, the body of the snake contorts into a curved pattern. By forming its shape into a curve, the snake then allows itself to continue to extend and contract until movement occurs. This continuous pattern allows the snake to slowly inch forward along the ground. In addition, by pressing against the wall or channel, the snake can use its muscles to propel itself from the surface, granting further movement through the area. Here,

while the snake continues to encounter frictional forces from the ground, it can counter those forces by using the walls as a counter force.

Serpentine locomotion is the movement that occurs when the body travels into different curve-like patterns. This motion is commonly associated with snakes that typically live in grassland areas or similar terrain. In serpentine locomotion, the head leads the motion of travel while the rest of the body follows the same path of the head. This motion, therefore, gives the appearance of the snake smoothly gliding through the given terrain. In addition, due to the body following the pattern set by the head, the snake is able to quickly start and stop their locomotion. Serpentine locomotion is dependent upon muscles projections against the ground on which the body lays against. In addition, the propulsion generated by the muscles in the snake results in lateral thrusts. These thrusts can grasp onto uneven surfaces, perpendicular to the relative motion, and can propel the snake to even further distances. Since this pushing motion is required for quick and sudden movements, the muscles in the body must generate enough thrust to compensate for the frictional forces acting against the body [14].

Sidewinding, or crotaline, locomotion occurs when the snake moves over a universally flat and smooth terrain. Some examples of a flat terrain would be sand, carpet, or other similarly textured surfaces. Crotaline locomotion is commonly considered a mixture of both the serpentine and concertina locomotion modes. For example, in crotaline locomotion, the entire snake is in constant motion, similar to serpentine locomotion. During crotaline movement, at least two of the three sections of the snake's body (head, middle, tail) remain parallel to the direction of movement. The other remaining section travels in curves similar to those found in the concertina movement. Due to this, the body moves in a diagonal direction rather than moving directly forward. The segment of the snake that is moving is lifted and becomes the main source of

propulsion. Since each section of the body is raised and then lowered, the snake quickly and suddenly hurdles forward. Since the snake cannot take advantage of uneven surfaces or walls to support and propel from, the snake must use its own body as a force of motion [14].

Rectilinear locomotion occurs in larger snakes such as vipers, anacondas, or pythons. Unlike the other three cases discussed above, where the snake relies on its curves to propel itself forwards, this type of movement occurs when the snake traverses in a straight line. In this form of locomotion, the snake seems to take physical steps. Small parts of the body of the snake lifts off of the ground and then places itself slightly further than where it once was. Due to the anisotropic frictional properties of the scales, the scales do not slide from their new position, acting as a non-slippery gripping surface. Due to this, the snake is then able to pull the rest of its body to the new position dictated by the lifted section. This pattern continues, allowing the snake to slowly move itself along in a straight line. Here, the muscles of the snake do not propel but instead are used to pull its own body weight [14].

This research focuses on the anti-slippery properties that occur on snake skin due to the anisotropic texture patterns found on the macro structure of snake skin. As the direction of movement effects the anisotropic nature of each scale, it is important to take into consideration how the variety of potential locomotional patterns increases or decreases the resulting frictional effects.

### 2.5 Downselection

For this study, it was decided to study the snake species *Python Regius* or the ball python. This species of snake is native to West and Central Africa and is found in the grassland and forest biomes. Ball pythons, which is the smallest species of python, are typically between 1 to

1.5 meters in length once adulthood is reached and can weigh between 4 to 5 pounds. Ball pythons received their name due to their habit of curling into a ball when threatened by a predator or other danger. This ball shape discourages predators from attacking the python, as the shape makes it harder to digest. In addition, coloring of the ball python ranges from different shades of brown. This allows them to camouflage and hide from their predators. Since the *Python Regius* is from the python family, it has a triangular head that gives the appearance of litheness while in actuality, the body of the snake increases in stockiness.

Ball pythons use a combination of rectilinear locomotion and serpentine locomotion. Due to its stocky structure and weight, it needs to rely on using its muscles to propel itself along surfaces. Therefore, the heavy middle of the snake carries most of the weight during locomotion.

Ball pythons nest in burrows or in other holes under the ground. Due to the constant travel in the burrows, the skin is constantly rubbed by dirt, sand, and other particulate matter. The *Python Regius* snake skin is subjected to severe wear in its harsh, underground environment and was therefore chosen to be the snake of interest for potential tribological applications. Since the shed snake skin shows the effects of the particulate matters on the scale texture design, it is optimal to study their ventral scales for their anisotropic frictional properties.

### 2.6 Summary

In this chapter, the basic anatomy of snake scales and their design were studied. Both the macro scale and micro scale textures that naturally occur on the scales were noted, studied, and analyzed in depth. Of particular interest were the directional u-shaped denticulations and fibrils that surround the surface of each macro scale, as they are the root cause of the snakes ability to trasverse. This hierarchical texture morphology plays the key role in the snake’s locomotion and

ability to traverse by providing anisotropic friction management and was explored experimentally.

# Chapter 3

## Design of Snake Scales

After understanding the hierarchal structures found on snake skin, a 3D sample model was developed and then manufactured using metal 3D printing. This chapter focuses on the design and creation of the modeled scales and their subsequent manufacturing.

### 3.1 Profilometer Scans of Snake Skin

To determine the dimensions of each type of scale on a snake, profilometer scans of the snake skin sample were taken. A Keyence VK-250 laser microscope (Elmwood Park, NJ, USA) was used for the images. Figure 6 shows a photograph of the equipment and setup.

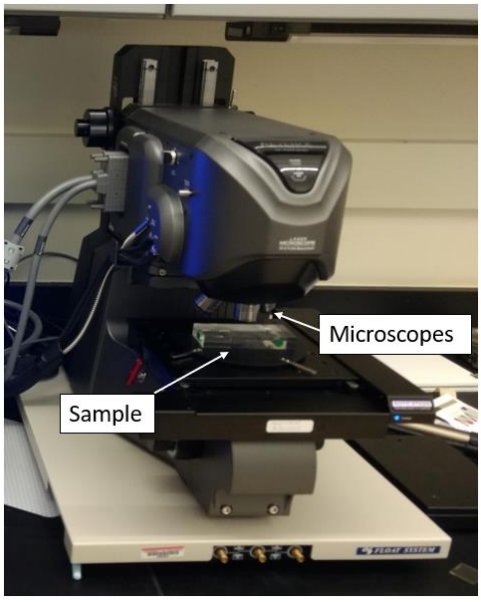


Figure 6. Visual of the Keyence VK-250 laser microscope tool (photo by author).

The Keyence laser microscope is capable of performing profile, roughness, and thickness measurements while remaining non-contact with the substrate to be tested while additionally providing the results in a nanometer resolution according to the manufacturer's website [15].

While other laser scanning microscopes, such as interferometers, have trouble reading reflective surfaces, the Keyence does not have this problem. This was a major reason the Keyence was chosen to perform the scans, as the snake shed is partially reflective and even clear in color as the shed does not hold the pigments in excess.

Another benefit to this technique is its non-contact measurements, ensuring that the shed skin isn't damaged. The shed skin that was commercially purchased already had some basic wear and tear along the shed itself. This was due mainly to the natural shedding process of a snake, as the shed is normally rubbed up against rocks or other materials to peel off the shed from a snake's body. Since the integrity of the shed was crucial to this experiment, a technique that could provide data on the surface of the skin without causing additional damage was crucial for the analysis.

To operate the laser microscope, the system combines a laser light source with additional white light. By combining these two light sources, the machine can both scan and collect data on the surface of the material. This gives access to both an optical image and the height information within the measurement area as the sample is scanned in both the X and Y directions during the measurement. The intensity of the laser itself also has an important role to play. The peaks and valleys found in the height profile can be measured by determining the intensity needed for the laser light to both go to the surface and get reflected back to a specific point on the machine. The raw data during the measurement is stored in the form of height information within the XY area which can then be used to calculate roughness values and other relevant surface texture parameters with the help of a software program.

The surface profilometer scans were intended to study the basic textures found on the ventral skin while providing valuable information about the hierarchical features in snake skin.

However, during the surface profile measurements, some challenges were encountered. Additional measures were taken to ensure and overcome these challenges as described below. The most common challenge was fitting the snake shed on the measurement area itself. The snake shed itself was very flimsy and would not lay flat onto the measurement area which is crucial for accurate surface profile measurement. Due to this, the shed skin was gently stretched out and anchored to the ends using suitable weights

In addition, the texturing found on the scales were visually clearer due to the taut positioning of the skin. The resulting scans of the snake shed using the profilometer are found below in Figures 7, 8, and 9.

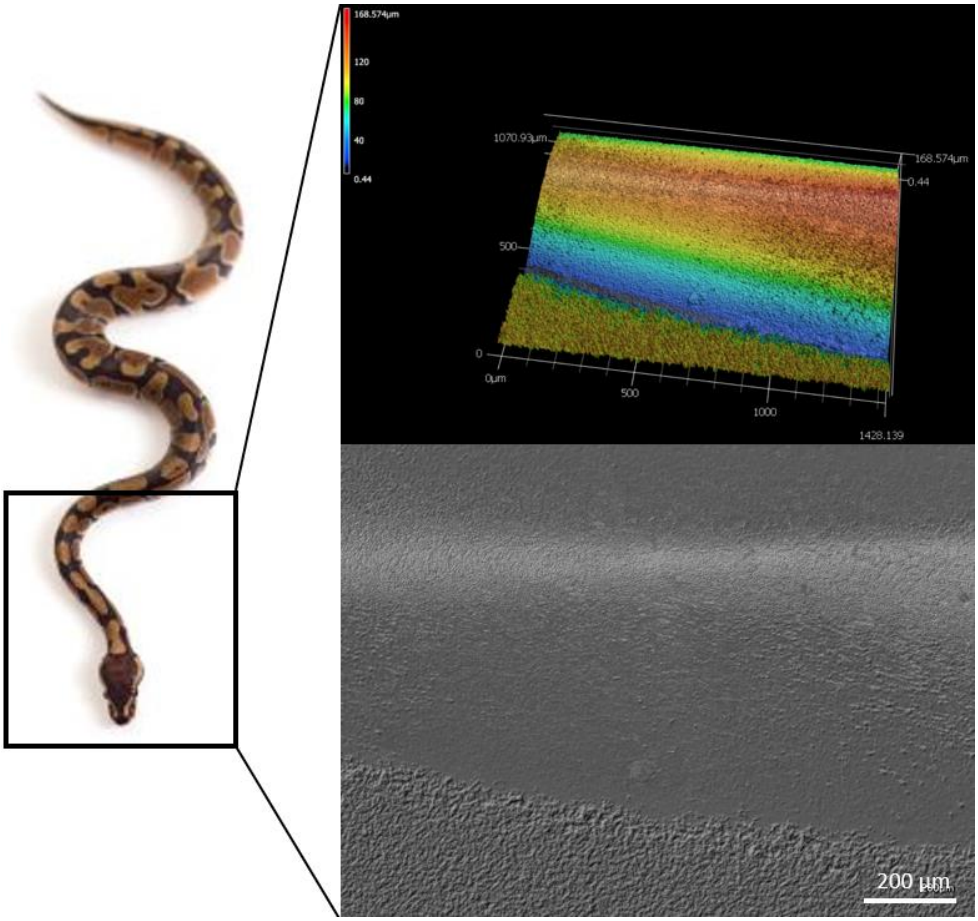


Figure 7. Profilometer scans of the natural snake skin at the head.

Figure 7 represents the ventral scales closer to the head of the snake. These head scales shown in Figure 7 are relatively smooth when compared to the scales measured on others regions of the snake's body (Figures 8 and 9). This is due to the head of the snake being the leader of locomotion, allowing for the skin to suffer less damage during movement. Since the head is the leader of locomotion, it is usually slightly raised and therefore, is not affected by the mating ground surface in comparison to the other sections of scales.

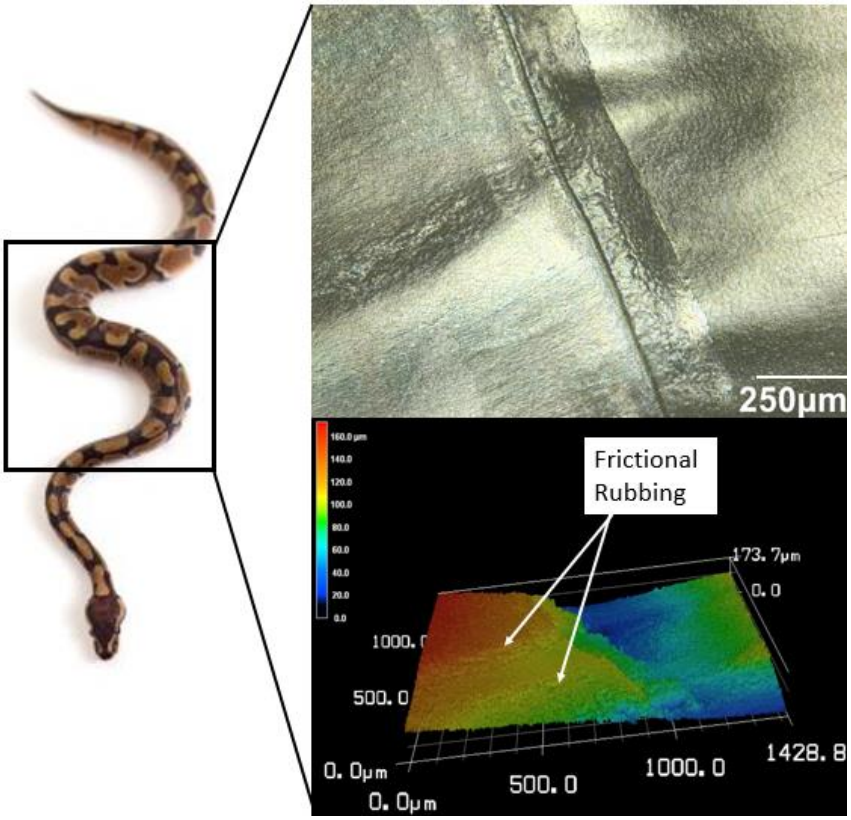


Figure 8. Profilometer scans of the natural snake skin at the middle ventral scales.

Figure 8 represents the ventral scales found on the belly of the snake. In comparison to the ventral scales found on the head, the ventral scales in the middle of the body show intense rubbing and frictional deformation. Figure 8 shows some of this wear and tear due to the effects of the rubbing.

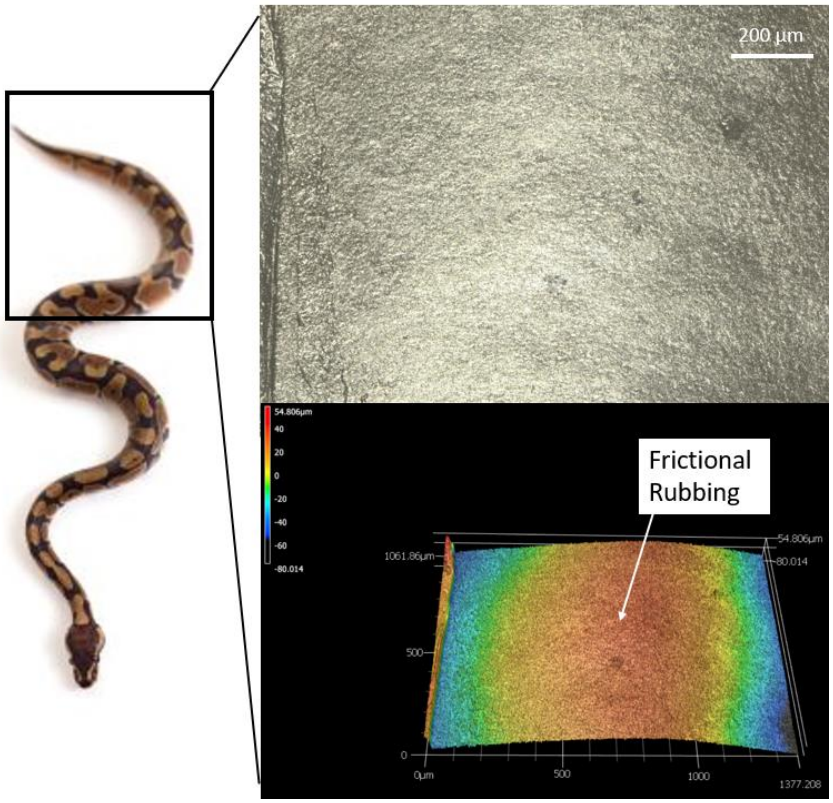


Figure 9. Profilometer scans of the natural snake skin at the tail.

Figure 9 represents the ventral scales closer to the tail of the snake. These scales also show some wear and tear due to how the tail of the snake is constantly in contact with outside forces. This wear and tear takes form in the shape of a rough and bumpy exterior. This exterior is quite prevalent as pointed out in Figure 8 where it is possible to see the rougher edges take shape due to the contact of the skin with the ground. Since the tail does not lead locomotion and always follows, it is constantly rubbed against other mating external surfaces as it trails behind and, therefore, can also show signs of this wear.

### 3.2 Proposed Design

As mentioned previously, the skin of a *Python Regius* was chosen due to the harsh environments the skin is subjected to while demonstrating advanced locomotion and related anti-

slippery properties. In addition, ventral scales were the focus of this research instead of the smooth outer dorsal scales. This choice was due to the fact that ventral scales hold the weight of the snake during locomotion, causing the frictional management to be highest among those scales and, thus, are relevant for the studying of the frictional management and manipulation properties of the snake skin for the fabrication of inspired surfaces. The ventral scales of a snake are also larger in size when compared to the dorsal scale counterparts, which gave a size advantage for modeling, fabrication, and controlled testing.

Commercially purchased (Etsy, Brooklyn, NY) shed snake skin was used to study, design, and model the sample for fabrication. The sample was received washed and cleaned, ensuring any contamination that might have been on the skin was removed. Figure 10 shows the optical view graph of the purchased snake skin.

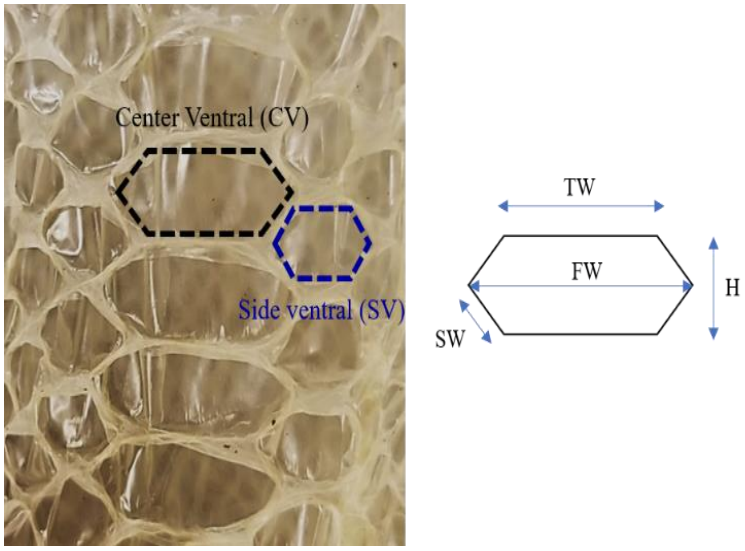


Figure 10. Snake skin sample and measured dimensions (photo by author).

As discussed above, to accurately model the snake skin for the purpose of experimental study and analysis, it was decided to measure the dimensions of the scales from an actual snake

specimen. Figure 10, a photograph, only shows the ventral scales of the skin purchased as it was the area of interest to this study.

The hexagonal patterns on the ventral scales were measured with a ruler. Using a sample size of about five ventral scales, the dimensions of a typical scale were calculated. In addition, eight side ventral scales, which are those bordering the central hexagonal ventral scales were measured as well. Both of the scales are depicted in Figure 10. Since these side ventral scales, intermittently, are also in contact with the mating ground surface, they were also included in the dimensional analysis.

Table 1 shows the averaged results of measurements for the ventral scales. These values were then used to design and recreate the average scales sizes that typically occur in a *Python Regius* species. As seen in Figure 10, each scale is separated by a small membrane. This membrane connects the scales together and also plays a major factor in the natural lubrication produced by the snake and the shedding process as well [10]. It also allows for the snake to stretch and shrink its body as needed for locomotion [16]. This membrane, or separation between each scale, was estimated and included in the dimensional analysis.

Table 1. Measurements of an average ball python scale size.

| | **Central Ventral** | **Side Ventral** |
|---|---|---|
| **Height (mm)** | 4.2 ± 0.8 | 3.1 ± 0.3 |
| **Full Width (mm)** | 10 ± 0.1 | 4.375 ± 0.7 |
| **Side Width (mm)** | 2.15 ± 0.23 | 2 ± 0.4 |
| **Top Width (mm)** | 7 ± 0.1 | 2.2 ± 0.4 |

Once the dimensions of typical central-ventral and side-ventral scales were determined, a 3D model of the snake scale was then be created in SolidWorks. The above measurements determined the overall size, shape, and distribution of the hexagonal patterns. A CAD drawing of snake skin inspired design based on the measurements (Table 1) is shown in Figure 11. The design, arranged for accuracy and likeness, is similar to the hexagons observed on the shed skin acquired. As mentioned previously, a sample size of five central ventral scales (~10 mm width) and eight side ventral scales (~4.375 mm width) geometry was measured. This was to ensure a large sample size of scales was created for controlled lab measurement. Typically, in nature, each scale is not exact in size in shape. The central ventral scales were measured to be about 10 mm long with a height of 4 mm whereas the side ventral scales were about 2 mm in size in each direction. The membrane width was measured to range at an average of 0.47 mm. As a total unit, the sample coupon measured to be around 25 mm long and 20 mm wide.

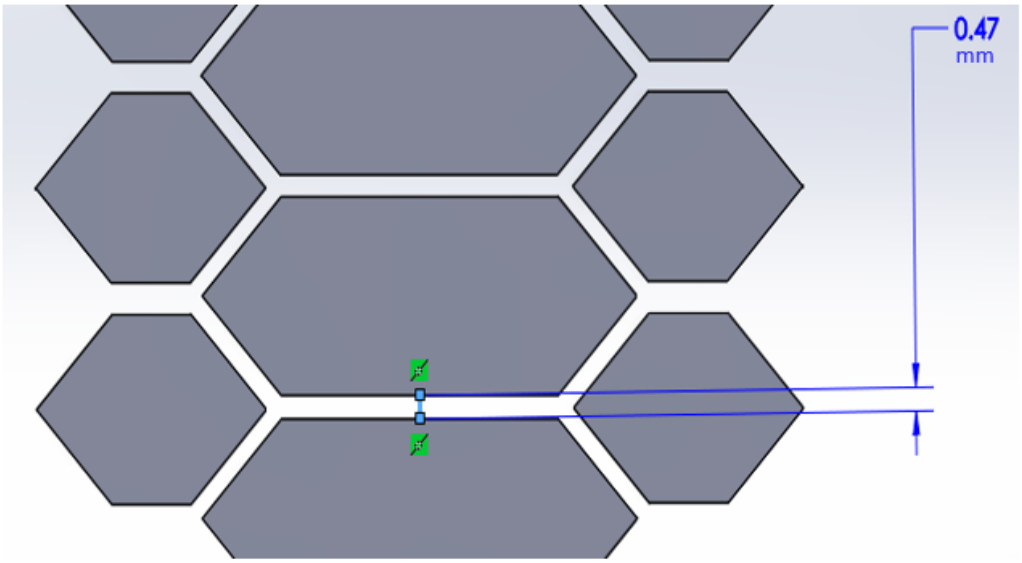


Figure 11. SolidWorks® model of snake skin.

### 3.3 Laser-Powder Bed Fusion Process

The additive process is a bottom-up manufacturing process in which material is used to build up many different layers. This process allows for near-net shape processing of the parts. The bottom-up process is commonly being used for the creation of prototypes as it is a quick and convenient process, hence its use for this project. In addition, the laser powder bed fusion process (L-PBF) process used in this work is capable of using the powder to print different materials such as metal, utilized here, but also plastics and other polymers. The L-PBF process is beneficial as it does not require a mold to print and can manufacture parts solely based on 3D design software.

In particular, to manufacture the snake skin design, a powder based additive manufacturing technique designated L-PBF (University of Louisville; Concept Laser MLab, Grapvine, TX) was utilized. In this process, a Concept Laser Mlab Cusing R laser (maximum power 100 W, coater type V-blade, Yb fiber laser, wavelength of 1050 nm) is scanned in X-Y plane to sinter powdered material at laser focus in a layer-by-layer fusion process. A 3D model shape is printed and sliced into multiple layers with the help from software. Each individual layer is then selectively fused with the help of a scanning laser pattern. The laser is capable of heating the powder locally to a temperature where the individual powder particles are fused together to create a specified shape. More powder is then placed on the material and the process repeats itself until a desired thickness and pre-planned designed is reached. Due to the existing 3D base model of the skin texturing, the laser can be utilized to trace the specific patterns. The movement of the laser scanning paths naturally results into u-shaped patterns much like those micro textures on snake skin, allowing for limited, to no, post processing to be required on the part, based upon observations from this work.

L-PBF process allows for a build size of a 90 x 90 x 40 $mm^3$ sample. The machine has minimum print dimensions of 10 microns in the z direction and 200 microns in the x and y directions. For this process, four parameters are needed to define the total amount of energy, 90 W, needed to sinter the powder on the material. These parameters are as followed: thickness of the layers, 20 µm; type of material, stainless steel 420; scanning speed, 600 mm/s; and, trace width, 120 µm. One benefit to this process, as mentioned earlier, is the laser scan pattern. The laser is scanned along a specified scanning pattern. Formation of a localized melt pool combined with the scanning pattern of the laser resulted in collective formation of macro and micro texture patterns on the surface which closely resembled the scales and directional denticulations observed on the snake skin.

Stainless steel is a commonly used engineering material for a variety of industrial applications and, thus, AISI 420 stainless steel was chosen to be the base material for the L-PBF process. In addition, due to its strength, hardness and other engineering properties, it was an appropriate choice for frictional management studies.

### 3.4 Fabrication of 3D Printed Model

To ensure that the fabricated pattern was smooth and continuous, as determined by the capabilities of the L-PBF process, a thickness of 100 microns was chosen. This choice would allow for the directionality of the laser patterns to remain consistent while also providing enough thickness of the printed layers (z-resolution = 10 microns) to ensure reproducibility of the printed texture. Multiple of these patterns were printed together as shown in Figure 12, allowing for consistent samples for testing. To fully separate each pattern from one another, a space of 10 mm was used. This was done to allow for sectioning of individual sample coupons needed for the experiments.

As seen in Figure 13, the sintering of the material by the laser was set perpendicular to the width of each hexagon. Due to this process, the directional texture found on the snake skin could be mimicked as the laser pattern naturally creates these textures due to its scanning movement.

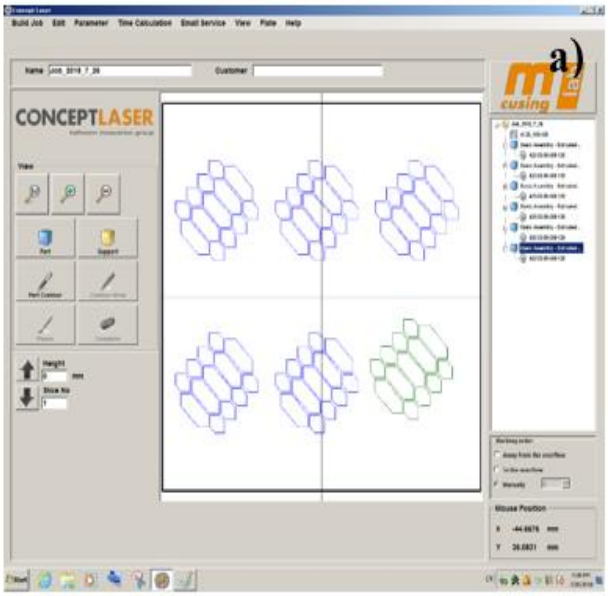


Figure 12. Concept laser printing outline (image courtesy: Subrata Deb Nath).

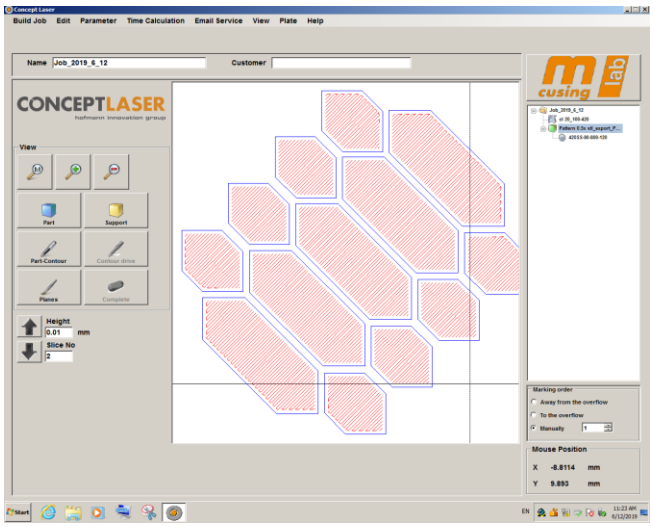


Figure 13. Concept laser printing full pattern (image courtesy: Subrata Deb Nath).

The printed samples were used without any further post processing in order to avoid any changes to the printed snake skin inspired texture. Figure 14a shows the entire coupon of printed structures while Figure 14b is a close up of one printed structure.

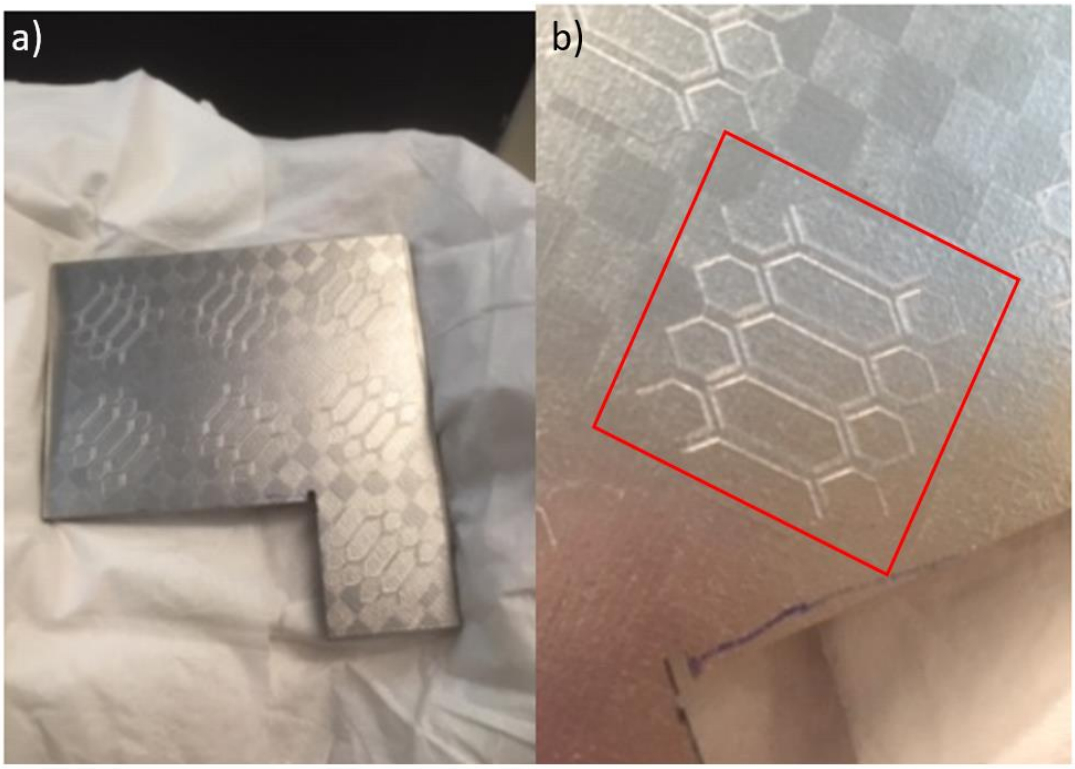


Figure 14. 3D modeled (a) complete and (b) individual coupon (photo by author).

The 3D printed parts were then characterized using a laser microscope (Keyence VK-250) for roughness and pattern comparisons between the snake skin and 3D printed steel samples.

### 3.5 Profilometer Scans of Sample Feasibility Study

After the creation of the first prototype scales, profilometer scans were taken to determine the dimensional accuracy of the prints as well as the surface texture and roughness measurements. Figures 15a and 15b show the representative scans of the printed parts in two

regions; (a) within the hexagonal scale and, (b) near the boundary of 3 different scales, highlighting the membrane area.

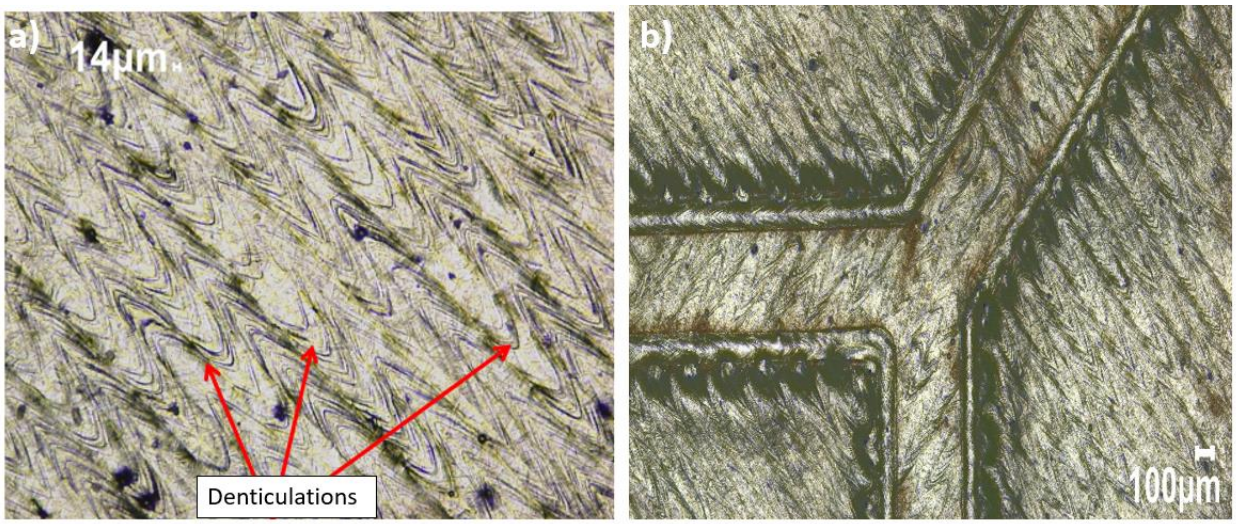


Figure 15. Profilometer scans of (a) the middle of a stainless steel scale and, (b) the membrane area.

As seen in Figures 15a and b above, there are clear u-shaped patterns throughout each scale much like the snake skin texture. Therefore, we can conclude that the L-PBF process was successful in creating the artificial denticulations. They were similar in both shape and size when compared to those observed on the actual snake skin shown in Figure 4.

The texture on the snake skin and the 3D printed sample were measured using the same Keyence VK-250 laser scanning microscope. The sample surfaces were measured at 10X magnification and the measurement data was analyzed using the Keyence multi-file analyzer software. For better accuracy in the profile measurements, line scan analysis was performed at five locations perpendicular to the texture orientation as shown in Figure 16; the average values are reported in Table 2. Profile roughness comparisons were made according to the ASTM surface roughness standards (JIS B 06061-2001).

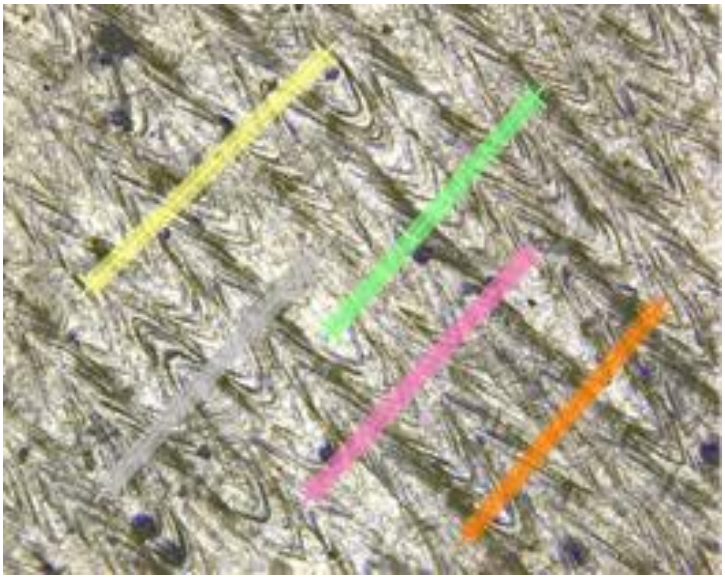

Figure 16. Line scan analysis performed on stainless steel sample.

Table 2. Comparison of selected profile roughness values measured on snake skin and 3D printed steel sample.

| | **$R_a$ (µm)** | **$R_{sm}$ (µm)** | **$R_q$ (µm)** |
|---|---|---|---|
| **Snake skin** | 7.32 ± 2.7 | 87.6 ± 53.3 | 8.82 ± 3.1 |
| **Steel sample** | 3.8 ± 0.78 | 142.22 ± 64.7 | 4.75 ± 0.7 |

In the measurements, $R_a$ represents the arithmetical mean height, $R_{sm}$ the mean width of the profile elements, and $R_q$ the root mean square height. These two parameters where chosen to be high priority when comparing the two different samples. Since $R_a$ and $R_q$ are used to determine and analyze the surface finish and, therefore, roughness on samples, it can be utilized to determine the deviation in heights on the denticulations with respect to the overall mean height of the denticulations. Here, $R_{sm}$ represents the mean distance between the repeating features. It allows for one to characterize the periodicity of the features in certain directions on the samples. This data is also useful to determine the repeatability of the printed pattern across

multiple locations. For all samples, the tilt of each sample was corrected before determining the values of the texture parameters.

Both $R_a$ and $R_q$, characterization values that determine the surface roughness, varied when comparing the natural snake skin to the 3D printed sample. In this case, the values on the 3D printed sample were larger in comparison. However, values were still comparable within given orders of magnitude observed on snake skin. Since the snake skin did not lie completely flat under the profilometer, this may have caused some of the discrepancies seen in the roughness averages. The low standard deviation observed on the 3D printed sample confirmed the repeatability of the texture pattern formed by the laser scanning. Thus, it could be concluded in the first order that with the 3D printing technique, better repeatability and control of the micro textures and denticulations could be deposited.

Similarly, the mean width, $R_{sm}$, of the profile elements was also larger in the 3D printed steel sample. However, once again, this value was comparable to that found on natural snake skin. As denoted earlier, this change was likely due to the shifting changes on the profilometer due to the snake shed not lying completely flat. Overall, when comparing both the surface roughness and width values, the periodicity of the profile itself was closely related to the pitch or artificially made denticulations between the many consecutive laser scan lines. This further indicated that it was possible to control the periodicity on the printed samples by controlling processing parameters.

Alongside the profile measurements, areal surface texture analysis was also performed on both the 3D printed steel sample and the natural snake skin according to the ISO 25178 standard [17]. Areal surface parameters were calculated over the measurement area as opposed to the line profile and, thus, convey more meaningful information about the functional properties of the

surface [18]. Since the snake will interact with the surfaces rubbed against its ventral scales through a contact area than a profile, the areal surface roughness values were critical to analyze. Typically, if the surface is course and rough, the surface of the sample will wear quicker causing higher coefficients of friction [18]. This is due to the fact that rougher surfaces resist the movement of objects causing the frictional coefficient to rise. Generally, the opposite can be said for smooth surfaces, in which lower coefficients of friction are observed. This tailored coefficient of friction effects skin-surface adhesion, which is determined by both the direction of movement and orientation and dimensions of fibrils and denticulations found on snake skin.

Table 3 shows the selected areal texture parameter comparison between the two different samples. For both measurements, at least five different areas of the snake skin and steel surface were considered. Due to the expected region-specific variability of the snake skin, this allowed negating any outliers that could greatly affect and skew the calculated results. $S_q$ represents the rms areal surface roughness standard [15]. The comparable areal surface roughness values measured on the printed steel surface thus confirm the feasibility of the 3D printing method to manufacture snake skin-inspired texture designs. Texture aspect ratio, or $S_{tr}$, represents the isotropic/anisotropic characteristics of the surface textures. A perfectly isotropic surface has a $S_{tr}$ value of 1 [15]. Since the $S_{tr}$ was less than 0.5 for both the steel surface and the snake skin, it could be concluded that both of the surfaces had directional texture present, as desired. Lastly, the final parameter, $S_{pd}$, could be used to calculate the density of the number of peaks per unit area. Similarly to the previous values, this parameter also remained comparable for both the 3D printed surface texture and the snake skin. Since the peaks could be viewed as contacting points with the counter-surface, $S_{pd}$ values were important for characterizing the tribological (locomotive) properties of the surface.

Table 3. Comparison of selected areal roughness values measured on snake skin and 3D printed steel sample.

| | **Snake Skin** | **Steel Sample** |
|---|---|---|
| **$S_q$ (µm)** | 6.37 ± 3.8 | 5.83 ± 0.94 |
| **$S_{tr}$** | 0.31 ± 0.11 | 0.47 ± 0.17 |
| **$S_{pd}$ (1/mm$^2$)** | 316970 ± 37789 | 85861 ± 1944 |

When measuring these textures, no post-processing was performed on the 3D printed sample. This was done to ensure that the naturally occurring denticulation texture was not changed due to post processing.

### 3.6 Summary

In this chapter, successful creation of a 3D printed model replicating the hierarchical macro and micro textures found on a snake skin was discussed. The texture parameters on both the natural scales and printed scale were analyzed. It was determined that the distribution of denticulations, the periodicity, and the aspect ratio were comparable between the two samples.

# Chapter 4

## Frictional Anisotropy Measurements and Analysis

Once the 3D printed samples were analyzed for the replication of bio-inspired texture designs, tribological testing was performed in order to study the frictional anisotropy. This chapter focuses on the experimental details for tribological results and their interpretation.

### 4.1 Experimental setup

As the goal of the experiments was to test if the 3D printed micro texture similar to those found on natural snake skin also results in frictional anisotropy (similar to snake skin), tribology testing was utilized. Figure 17 shows a photograph of the ball-on-disk tribometer (CSM Instruments, Graz, Austria) that was used to perform the friction anisotropy testing under a rotational mode to simulate unidirectional sliding motion. The instrument consists of a sample disc, a ball counter surface, load weights, and balancing weights.

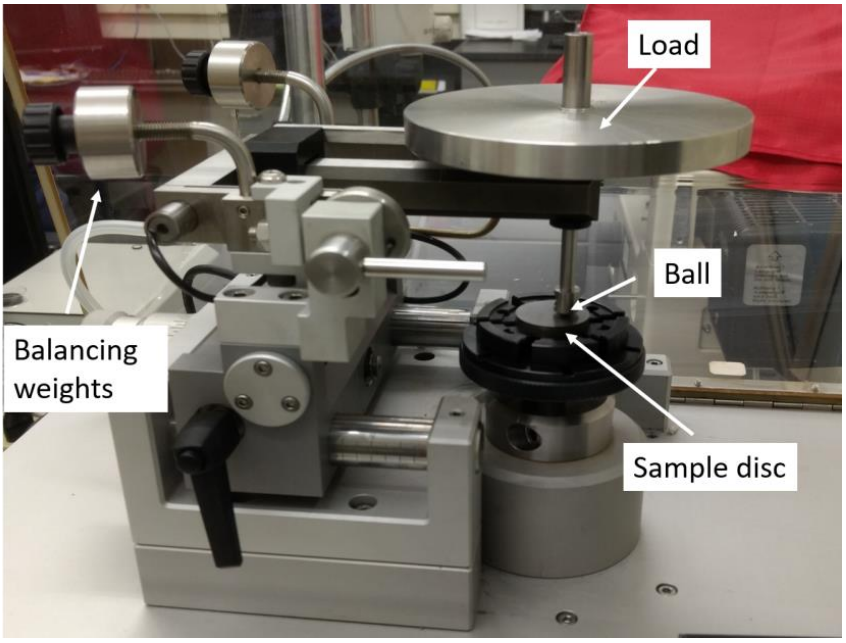


Figure 17. Ball-on-disk tribometer experimental set-up.

A ball-on-disk tribometer is an instrument designed for tribological characterization. Primarily, the machine simulates the point contact loading (under rotational or reciprocating modes) and is a commonly used testing setup for performing scientific research. The machine is capable of providing results at two interacting surfaces, for example with lubricants or other material coatings. The tribometer used for these experiments included a ball that was loaded against a sample disc that rotated around in place. Mirror finished grade 52100 hardened steel balls (McMaster-Carr) were used as a counter-surface. This ball tip – sample contact simulated the contact between the snake skin texture and a rough terrain surface under unidirectional sliding. Once the contact was made between the ball and 3D printed steel sample textured surface, the coefficient of friction could be determined by comparing the frictional force experienced to the loading force applied by a weight on the ball itself.

To run the experiment, a few steps needed to be completed prior. The tribometer setup allows mounting of circular discs clamped by concentric jaws. The 3D printed steel samples, on the other hand, were square in shape. To counteract this problem, based on the recommended procedure from CSM Instruments, the manufacturer, the 3D printed square sample was glued on circular discs for mounting.

Another step that was crucial to the experiment was the proper alignment and orientation of the sample with respect to the rotational movement of the ball. This was important to simulate the unidirectional sliding motion to test frictional anisotropy with respect to orientation of the micro texture. Figure 18 illustrates the alignment that was followed during the experiments and represents a serpentine locomotion pattern. As shown in the figure, the movement of the ball followed the directional pattern of the printed part at different relative orientations. In Segment I (yellow), the ball moved parallel to the orientation of the micro texture, akin to a snake traveling

in a straight forward direction alongside the denticulations also oriented parallel to the direction of movement. It is in this sectional that friction was anticipated be lowest as the movement was going along micro texture. In Segment II (green), the ball moved away from the forward direction, akin to a snake's curves in locomotion generation. It is in this section where friction was anticipated to increase. In Segment III (blue), the ball motion starts to return to parallel, as and such, a frictional decrease was anticipated.

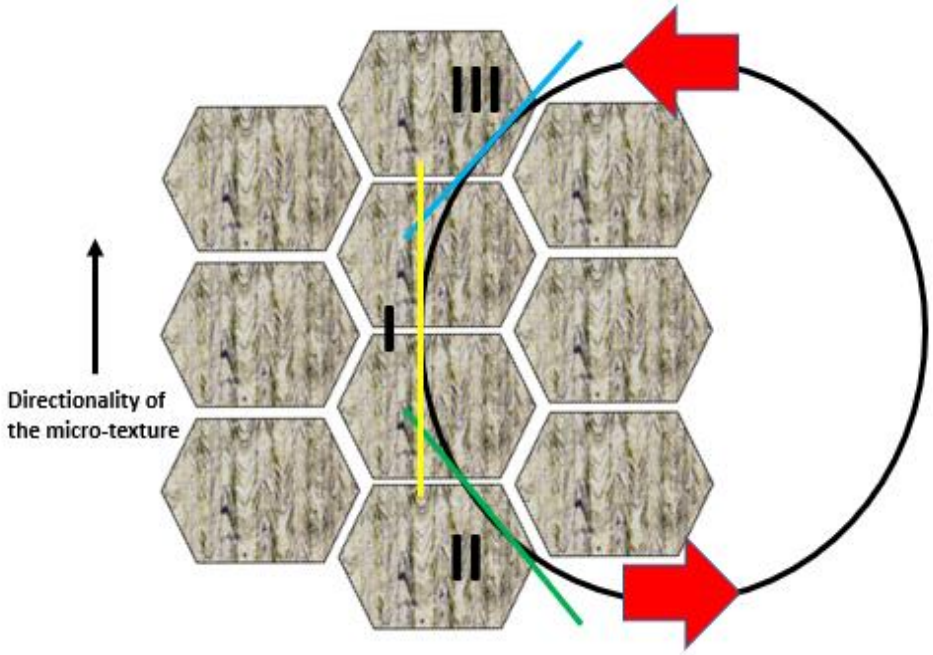


Figure 18. Outline of ball travel path.

As seen in Figure 18, this would allow for the directionality of the micro textures on the ventral scales to be tested in terms of their role on the friction manipulation. This circular and unidirectional path of travel allowed for the testing of the pattern while at various angles of locomotion. These angles were related to the angles found during serpentine locomotion discussed before in Chapter 1 (Figure 5). The anisotropic frictional properties could then be analyzed by determining the average friction at various occurrences in this circular path.

To make sure that no residue was left on the steel sample, the sample was cleaned with organic solvents. In the first of these processes, the sample was soaked in acetone in an ultrasonic bath for 10 minutes. The ball and the ball holder, which act as counter-surfaces in the tribometer, were also sonicated for cleaning. This process was used to make sure that all external particulates were off of the surface of the sample before testing.

Since the acetone would break away the adhesive that allowed the steel sample to be mounted on the disc, the positioning of the two was set up before the cleaning procedure. This was achieved by placing the steel sample onto the disc with the intended radius of rotation for the ball to determine the optimum position of the steel sample. The sample was then outlined on the disc using a sharpie. The directionality of how the sample was mounted was also noted and marked to ensure the proper orientation of the micro texture at the beginning of the test with respect to the ball. After sonication, the sample was mounted on a disc with the help of the adhesive by using alignment markings. The sample was then mounted into the tribometer to confirm that the sample was in the intended correct orientation as determined previously. If found that the sample had moved, the parts were soaked in acetone which would release the superglue and the process would be started over from the beginning again.

Once it was confirmed that the sample would follow the path similar to the motion outlined in Figure 18 above, the tribological test was started. After mounting the sample, 2-3 drops (sufficient to keep the contact lubricated during the test duration) of lubricant were placed onto the sample. Due to the future interest of eventually applying this idea in industrial and design settings, which include gears, rails, etc., commercial Super Tech 80w-90w gear oil (Middleton, Wisconsin) was chosen to be the lubricant of choice. After the lubricant drops were placed, the sample disk was rotated manually to ensure even spreading of the lubricant along the

rotational track. If the lubricant was not spread evenly and was not spread across the entire surface, frictional results could be skewed.

The balancing weights and load then needed to be set before the experiment could begin. For the first experimental test, a load of 15 N was chosen. This choice was made based on the average weight for an adult ball python snake. This load would best stimulate the amount of load that would occur on the snake skin as the snake traveled. Before applying the 15 N load, the setup was balanced to a 'zero load' condition with the help of balancing counterweights as per the standard operating procedure.

### 4.2 Experimental Details and Test Results

For the first experiment, a rotational speed of 30 cm/s was chosen. In addition, 100 laps, or full circles with radius of 6.5 mm, was chosen as the test duration. This speed was chosen due to the maximum speed a typical ball python snake could achieve. This would allow for the most accurate bio-inspired surface's friction tests. 100 laps duration was chosen as it would simulate the snake traveling over long distances (approximately 5 m), allowing for the testing of snake skin after it has been worn, similar to natural snake skin and how it breaks down over time due to rubbing against the earth.

Table 4. Repeat testing results.

| Test No. | Tribo-testing parameters | Duration of the test | Notes |
|---|---|---|---|
| 1 | 15 N, 30 cm/s | 100 laps | Initial test – Feasibility testing |
| 2 | 15 N, 1 cm/s | 500 laps | Testing at 1cm/s and at 500 laps |
| 3 | 15 N, 1 cm/s | 500 laps | Repeatability test |
| 4 | 15 N, 1 cm/s | 500 laps | Repeatability test |

Under the chosen tribo-testing parameters, Test 1 took about 10 minutes for the 100 laps to be completed. Once, the test was over, the sample was removed so that profilometer scans of the wear pattern could be done. The frictional results of the first test are shown below in Figure 19. In all coefficient of friction (COF) plots, the x axis represents the laps taken by the ball on the 3D printed sample and the y axis represents the unitless coefficient of friction.

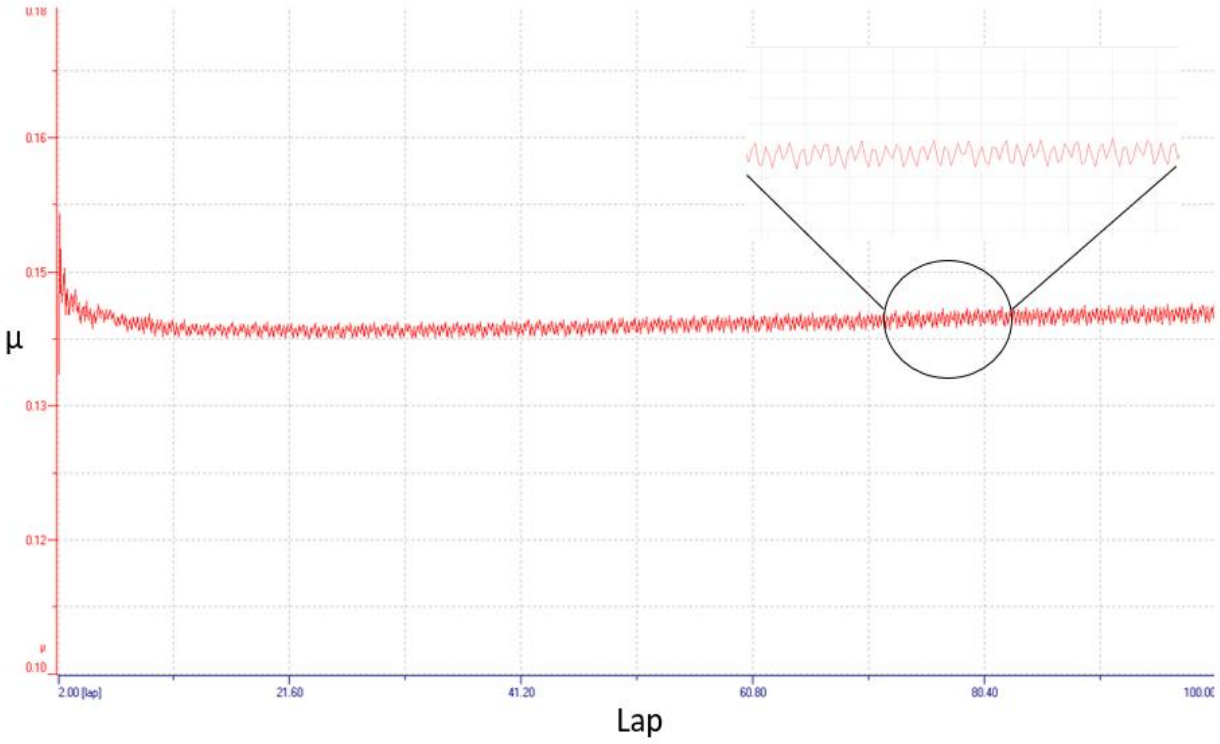


Figure 19. Tribology results of first test.

One of the first points to note is the periodic wave pattern with clear peaks and valleys that occured throughout the duration of the test. This pattern shows the effects of directionality of the micro texture on frictional anisotropy as the contacting ball entered and exited the texture pattern.

To take a closer look at this phenomenon, a schematic of the tribological testing track is shown in Figure 20. This track directly correlated the frictional response found due to the

tribological test.

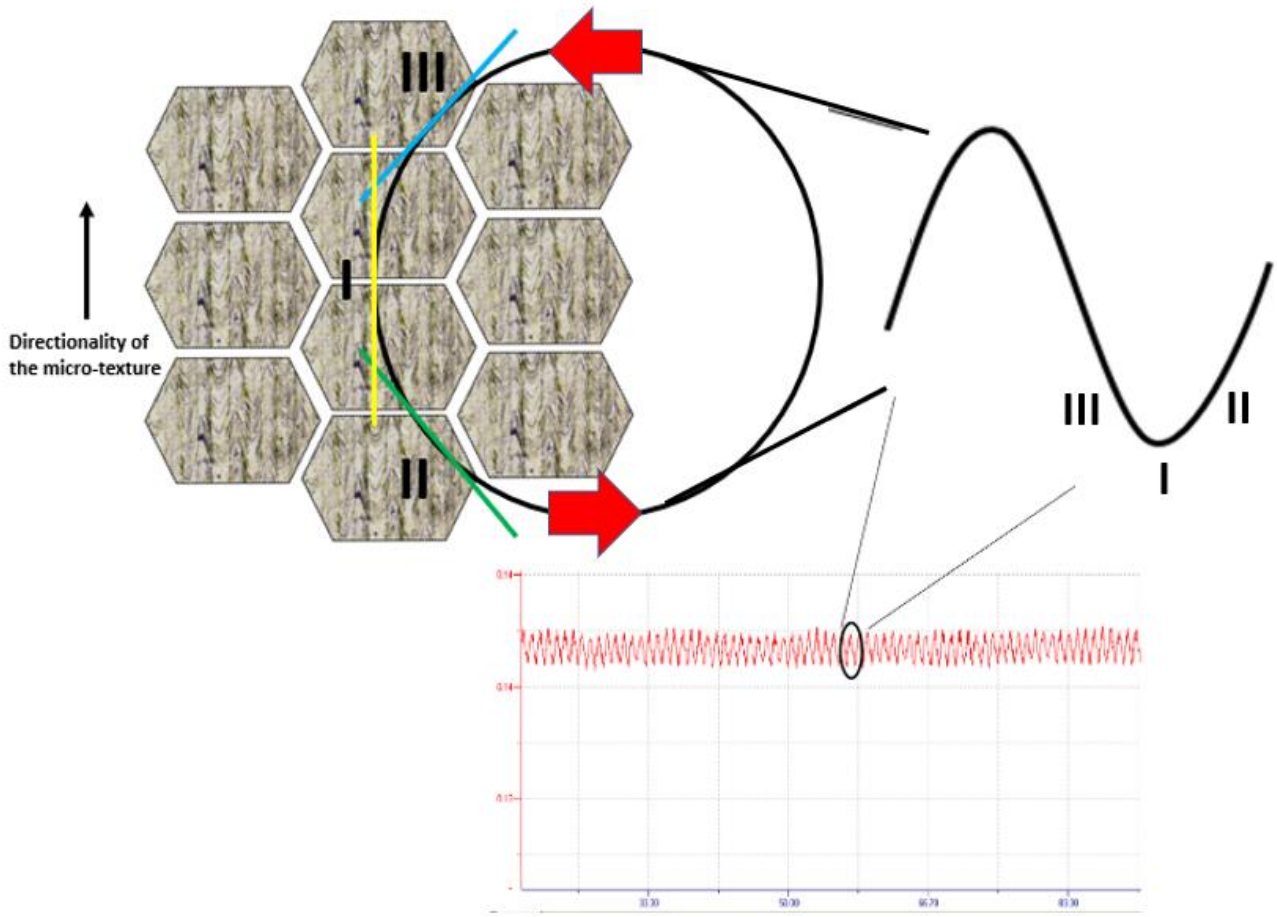


Figure 20. Oscillating pattern created by the tribology tests.

The testing track diagram was split up into three separate sections. Those are as follows: yellow (Section I), green (Section II), and blue (Section III). Each one of those sections corresponded to a specific directional movement of the ball with respect to the micro texture. The first section (yellow, I), as seen in Figure 20, corresponded to the lap segment where the movement of the ball was aligned with the micro texture pattern orientation. The second section (green, II) represents movement away from the pattern direction at an angle. Lastly, the third (blue, III) section represents movement toward the pattern alignment.

From those frictional testing results, the following important conclusions were drawn. First, the effects of directionality on the micro texture was clearly shown as manifested via oscillating coefficient of friction. Second, each part of the pattern can be directly correlated to specific points on the graph. In this case, the valley of the graph corresponds to Section I and represents the condition where the ball (counter-surface) moves parallel to the micro texture direction. As the ball moved along the micro texture with an angle, the COF increased in Section II before reaching its peak when the ball was outside of the hexagonal pattern. The COF started to drop down again as the ball moved closer to alignment of the micro texture in region III. The rise and fall of the peaks and valleys therefore corresponded to Section II and III, respectively. This behavior is similar to movement of a snake where directional denticulations ensure low friction for forward motion while resisting backward motion.

In this test, there was a clear pattern to friction force anisotropy as the ball travelled through micro texture's valleys and peaks through the three sections discussed above. Each valley corresponding to lower friction value on this COF plot represented the area where the counter-surface was aligned and moving parallel to the direction of the micro texture pattern. As the relative alignment between the counter-surface and the micro texture changed along the path, the COF increased. This was attributed to the ball moving relative to the orientation of denticulations. As the ball traveled with the pattern, the COF was at its lowest. As the ball moved away from the direction relative to the denticulations and into an angular direction, the COF increased. As the ball traveled against the pattern, the COF was at its highest due to the ball rubbing against the unnatural direction of the denticulations. As the ball traveled in almost a full circle, the COF once again started to decrease as the ball traveled back to be parallel with the denticulations. Therefore, a periodic increase and decrease following the micropattern's

periodicity was observed. This demonstrates that snake skin micro texture could control traction at microscale by periodic modulation of micro frictional properties of 3D printed steel sample.

To check the repeatability of the friction behavior, further testing was continued. Following the results of Test 1, it was noted that with the speed of 30 cm/s and at 100 laps, the test did not show a recognizable wear track on the sample due to the small test duration. Thus, for the next set of experiments (Tests 2-4), the stop condition was increased to 500 laps and the speed was lowered to 1 cm/s. Under those conditions (15 N, 1 cm/s), the experiment simulated boundary lubrication regime where the tribological surfaces are under direct contact. The same procedure, as described above, was followed for the subsequent experiments. The frictional results of the other tests are shown in Figure 21.

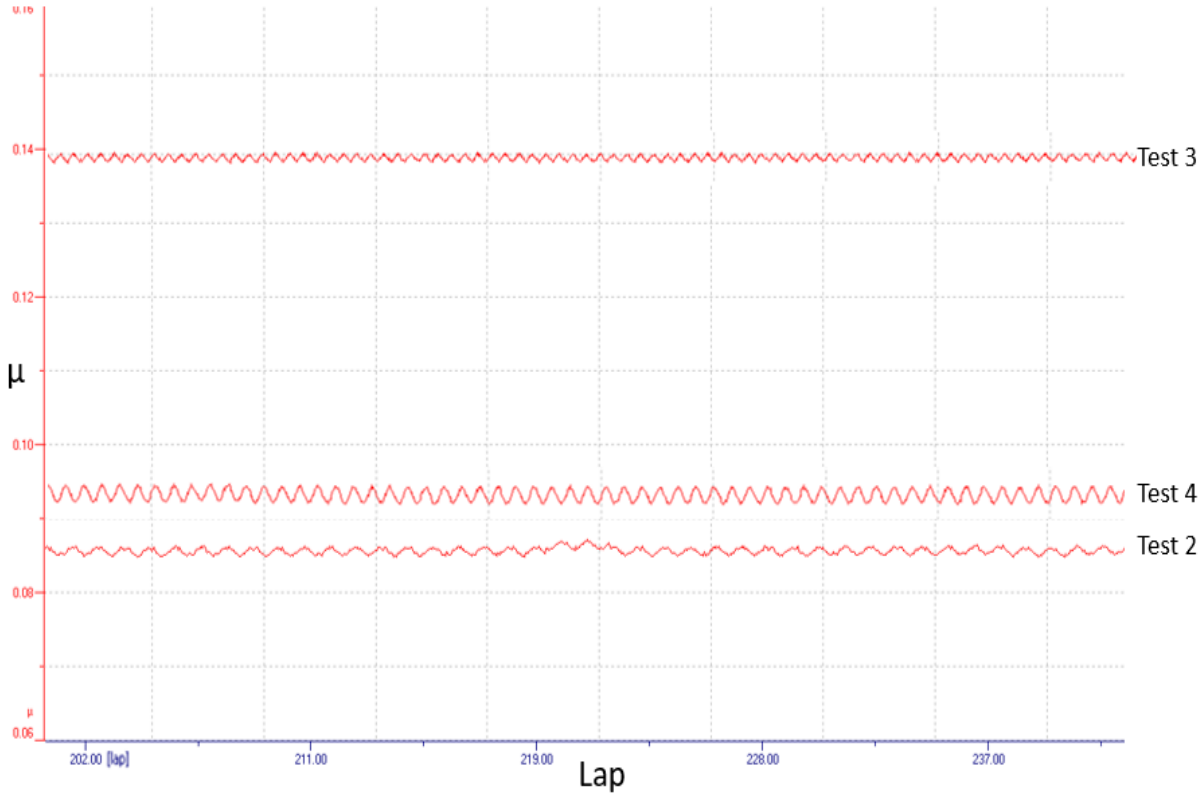


Figure 21. Tribology results of the repeatability tests (tests 2,3 and 4).

Overall, every test showed the periodic increase and decrease that represents the anisotropic friction behavior governed by the directionality of the micro texture. Similar to the results of Test 1 discussed above, all three repeat tests show anisotropic frictional response. Also, it should be noted that the periodicity in the sinusoidal friction plot (valley-to-valley distance) was one lap. This further confirmed that the locally changing orientation of the ball movement with respect to texture direction manipulated the COF. It is important to note that the COF for each test differed in value. However, the goal for the research was to show that it was possible to recreate the anisotropic properties found on snake skin. Therefore, the average COF was not as important as the amplitude and overall behavior of the pattern itself. These tests results therefore concluded that the snake skin micro texture affected traction at the microscale due to the periodic u-shaped denticulations in the 3D printed material.

To further prove this claim, the COF at different points in the circular lap was tested to show that this oscillating pattern was due to the texture on the sample. To further break down the oscillating pattern, the circular pattern was split up into five different sections. The orange section in Figure 22 represents the data points taken from when the ball was in the direction of the denticulations. The gray data was when the ball was moving away from the pattern. The yellow was when the ball was in the backward direction of the denticulations. And, the light blue and dark blue represents the data points taken when the ball left the backward direction and traveled toward the direction of the denticulations again. Data points were taken from all of the laps and were grouped based on their location into five sections. The grouped data, as summarized above and shown in Figure 22, represents the results of all of these points averaged in each of their respective sections. Therefore, the average COF within each section can properly be shown and be further inspected upon.

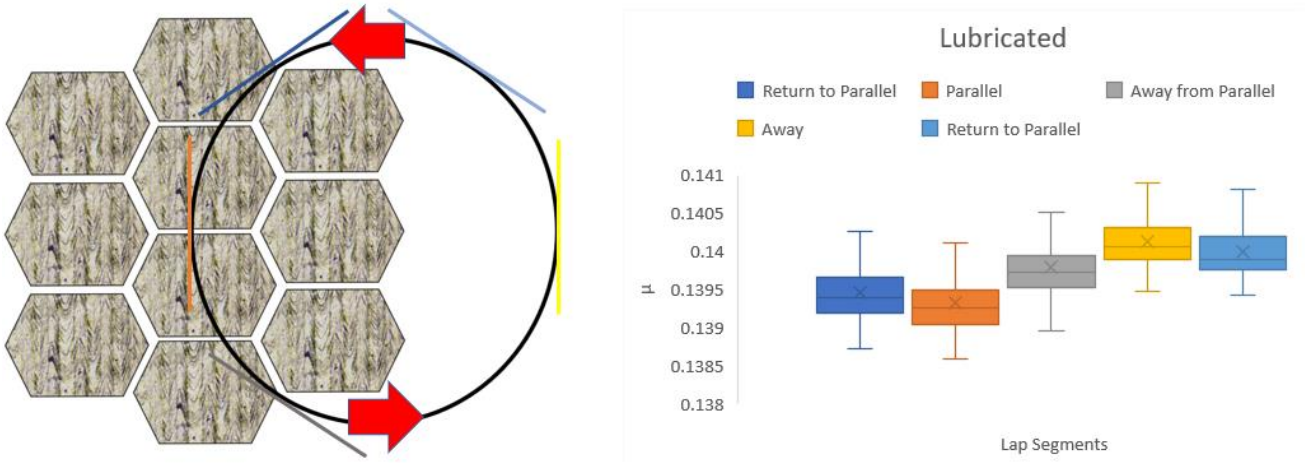


Figure 22. Data Representation of circular pattern.

There was a clear sinusoidal shaped pattern that backed up the finding that the u-shaped micro structure alone affected the overall frictional effects seen in all of the tests.

### 4.3 Effects of Hierarchical Textures

#### 4.3.1 Updated texture designs for studying role of hierarchical texture

The first tests discussed above showed anisotropic frictional properties and patterns on the steel sample. Therefore, it confirmed successful replication of snake skin pattern using L-PBF technique. In order to understand the role of hierarchical texture in snake skin (hexagons at macro-scale and denticulations at the micro-scale; Figure 23), the next set of experiments were focused on micro and macro scale textures individually.

To properly test the effects of the macro textures versus the micro textures, two alternate designs were created. These designs were similar to the original design and arrangement of hexagonal scales, but the overall dimensions of hexagons were scaled to a different size. The first design was sized to 1.5x the dimensions of the original pattern. In this design, the scales

were larger and allowed for the testing role of the microscale denticulations predominantly. The second design was sized to 0.75x the dimensions of the original pattern. Here, the scales were smaller and would predominantly test the effect of macro-scaled hexagons rather than the micro textures. Table 5 summarizes the next plan of experiments and the purpose of each as mentioned above.

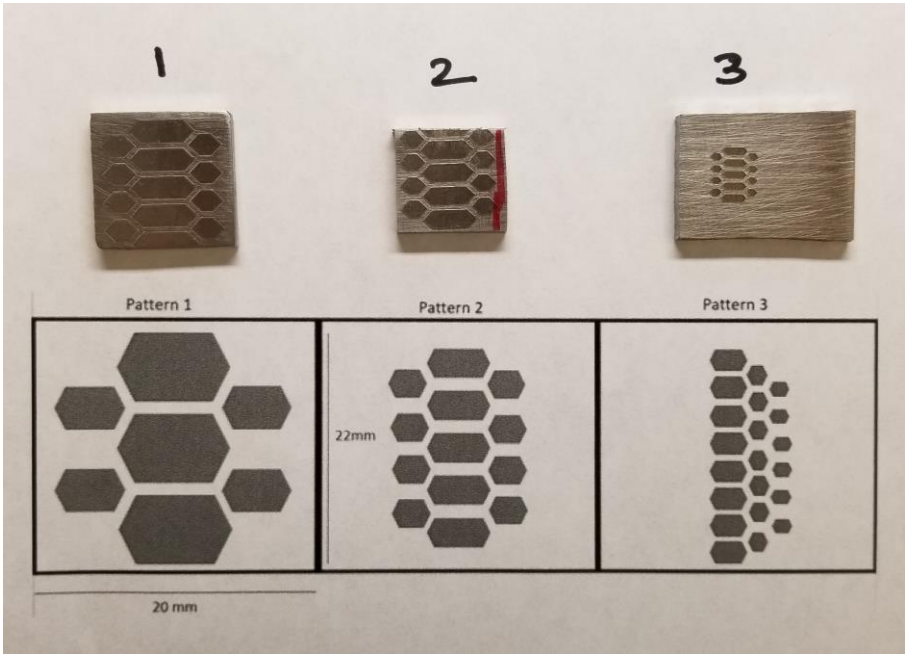


Figure 23. Schematic of the three patterns.

Table 5. Texture size parameter matrix.

| Pattern | Size | Notes/Purpose |
|---|---|---|
| 1 | 1.5x the size of the dimensions of the original pattern | Pattern to test the effects of the micro texture (denticulations) only |
| 2 | Original pattern and sizing as measured and tested previously (real scale dimensions) | Pattern to test the combined effect of the macro and micro textures like snake skin. |
| 3 | 0.75x the size of the dimensions of the original pattern | Pattern to test the effects of the macro texture (scales) only |

The scaling was chosen based on the planned technical goal and the capability of the L-PBF instrument in terms of printing the desired pattern. For the sake of brevity, the larger pattern for testing the micro texture will be dubbed as Pattern 1, the original pattern as tested in Section 4.2 will be dubbed as Pattern 2, and the smaller pattern for testing the macro texture will be dubbed as Pattern 3. The scaling of all three patterns are shown in Figure 23.

Once all patterns were fabricated, surface roughness analysis was conducted on all samples using the same roughness parameters and equipment discussed in Chapter 2. This would guarantee that although the dimensions and arrangement of hexagonal pattern on the samples were scaled to different sizes, the micro texture pattern dimensions remained consistent between all samples to allow for valid comparison between the three sets. The results of the measurements are presented in Table 6 below.

Table 6. Roughness comparison between the three samples.

| | $R_a$ (µm) | $R_{sm}$ (µm) | $R_q$ (µm) |
|---|---|---|---|
| Snake-Skin | 6.11 ± 3.8 | 162.7 ± 100.8 | 6.99 ± 4.03 |
| Large Pattern-1 | 2.55 ± 0.26 | 77.7 ± 9.22 | 3.3 ± 0.29 |
| Normal Pattern-2 | 2.95 ± 0.37 | 83.9 ± 22.3 | 3.82 ± 0.57 |
| Small Pattern-3 | 2.57 ± 0.26 | 76.2 ± 15.2 | 3.28 ± 0.32 |
| | | | |
| | $S_q$ (µm) | $S_{tr}$ (µm) | $S_{pd}$ ($1/mm^2$) |
| Snake-Skin | 19.61 ± 5.49 | 0.357 ± 0.12 | 82072.24 ± 11953.09 |
| Large Pattern-1 | 3.902 ± 0.16 | 0.19 ± 0.05 | 77293.02 ± 1566.81 |
| Normal Pattern-2 | 4.48 ± 0.17 | 0.207 ± 0.03 | 61215.62 ± 36968.75 |
| Small Pattern-3 | 4.7 ± 0.78 | 0.323 ± 0.08 | 93550.3 ± 4167.9 |

While the initial values for the $R_a$, $R_{sm}$, and $R_q$ on the snake skin were higher compared to the three steel patterns, they fell into the range of their standard deviation. Therefore, it could be

concluded that the steel and skin samples were comparable and could be used as an accurate model. These values were also closer in comparison with the previous results that were presented in Tables 2 and 3. A similar conclusion, in which the results of snake skin were higher than the steel samples, is shown by comparing $S_q$, $S_{tr}$, and $S_{pd}$. However, while the snake skin values were larger, the values for all three different sized steel patterns were similar. Due to this similarity, it could be concluded that the micro texture for each of the steel samples remained consistent even though the size of each scale differed.

### 4.3.2 Tribological testing results and discussion

Since the micro texture on each of the three different sized patterns was confirmed to be comparable, frictional analysis on each test was conducted to determine the effect of the macro and micro textures separately. For these tests, the duration was increased to 10,000 laps to ensure that the consistency of data across all the tested samples and allow for valid comparison between the varying macro-texture. The load and speed for the tests were kept same at 15 N and 1 cm/s as previous experiments discussed in Section 4.2. A summary of the tests conducted is shown in Table 7 below.

Table 7. 10,000 lap testing results.

| Test No. | Tribo-testing parameters | Duration of the test |
|---|---|---|
| Pattern 1 (Test 1) | 15 N, 1 cm/s | 10,000 laps |
| Pattern 1 Repeated (Test 2) | 15 N, 1c m/s | 10,000 laps |
| Pattern 2 (Test 3) | 15 N, 1 cm/s | 10,000 laps |
| Pattern 2 Repeated (Test 4) | 15 N, 1 cm/s | 10,000 laps |
| Pattern 3 (Test 5) | 15 N, 1 cm/s | 10,000 laps |
| Pattern 3 Repeated (Test 6) | 15 N, 1 cm/s | 10,000 laps |

The results of the tribological tests on the samples, as outlined by Table 7, are shown in Figure 24.

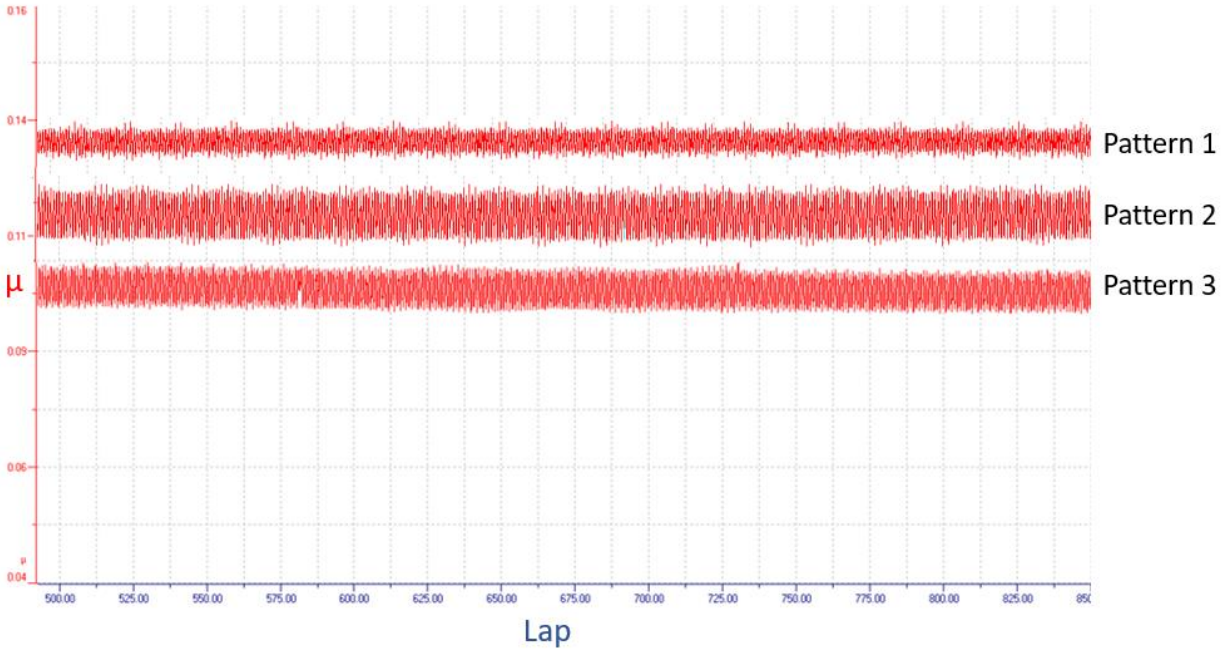


Figure 24. Comparison of tribological results from representative samples on the three tested patterns.

Each graph shows consistent sinusoidal pattern that was shown in the previous set of experiments, once again demonstrating that anisotropic frictional properties are delivered due to presented design on all three samples. To prove that anisotropy in coefficient of friction (COF) occurred due to the created micro pattern (representing the denticulations on the snake skin) and not due to the scales macro pattern (representing the hexagonal scales on the snake skin), the average amplitude of each curve and average full width half maximum (FWHM) was determined.

Each pattern was sampled at four different time frames to compare the amplitude and the FWHM of each test. These time frames were from 200-300 laps, from 3500-3600 laps, from

6600-6700 laps, and from 9500-9600 laps. It was found that the amplitude of Pattern 3 was the highest at an overall average of 0.0196, followed by Pattern 2 at 0.0114, and Pattern 1's amplitude was the smallest at 0.0088. These results demonstrate that the effects of the texture appear to be more apparent in Pattern 1 than in Pattern 3 and can be shown in Table 8.

Table 8. X/Y amplitude results.

| Pattern | Size | Laps 200-300 | Laps 3500-3600 | Laps 6600-6700 | Laps 9500-9600 | Average Amplitude |
|---|---|---|---|---|---|---|
| 1 | 1.5x Original Size | 0.00965 +/- 0.0018 | 0.00844 +/- 0.0015 | 0.0084 +/- 0.0014 | 0.0088 +/- 0.0014 | 0.0088 +/- 0.0005 (Max: 0.00965 Min: 0.0084) |
| 2 | Original Size | 0.0121 +/- 0.0031 | 0.01174 +/- 0.003 | 0.01056 +/- 0.0028 | 0.0112 +/- 0.0027 | 0.0114 +/- 0.0006 (Max: 0.0121 Min: 0.01056) |
| 3 | 0.75x Original Size | 0.0126 +/- 0.0028 | 0.0102 +/- 0.002 | 0.01104 +/- 0.0023 | 0.012 +/- 0.0026 | 0.012 +/- 0.0005 (Max: 0.0126 Min: 0.0102) |

Since Pattern 1was 1.5x the size of the original pattern, each individual scale was larger. Therefore, when the ball traversed its circular pattern, primarily the micro textures were evaluated as the ball was able to stay on the same scale and was not affected by the ball traversing from one scale to the next. Similarly, since Pattern 3 was 0.75x the size of the original pattern, primarily only the effects of the scales in the pattern were tested rather than the micro texture itself since the scales were not large enough for the micro texture to be properly evaluated. This further confirmed the hypothesis that the micro texture and denticulations were affecting the anisotropic and anti-slippery properties by manipulating friction at micro scale and not the overall scale size and the spacing between adjacent scales. This could be attributed to the fact that the textural effects were more prevalent in Pattern 1. In the larger pattern (Pattern 1),

the hierarchical texture itself dictates the increase and decrease of the COF. In the smaller pattern (Pattern 3), the increases and decreases in the COF were in part due to the ball traveling over the ridged space between adjacent scales or also called the 'membrane' that separates each scale.

### 4.3.3 SEM and surface profile characterization of the wear tracks

After frictional analysis was performed, SEM scans of the wear tracks were taken. These wear tracks were measured for consistency. It was found that the wear track was not continuous over all three sample patterns. This was due to the shape of the sample itself, as the patterning was not consistent. The ball traveled over the highest part of each one of the denticulations and did not make continuous contact with surface and, as such, parts of the wear track did not result. However, overall the wear track itself remained consistent in both size and shape. Figures 25 and 26 show SEM micrographs of the wear track for each pattern at magnifications of 500x and 2500x.

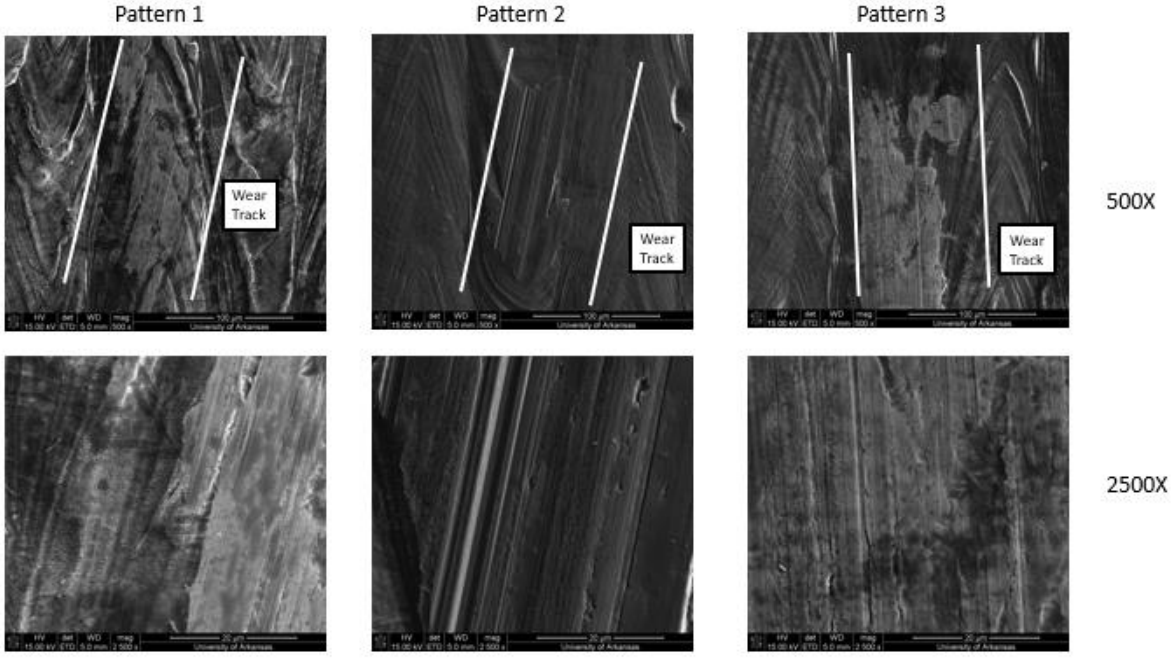


Figure 25. Wear track of all patterns at 500x and 2500x taken at a location where ball travelled parallel to the texture orientation.

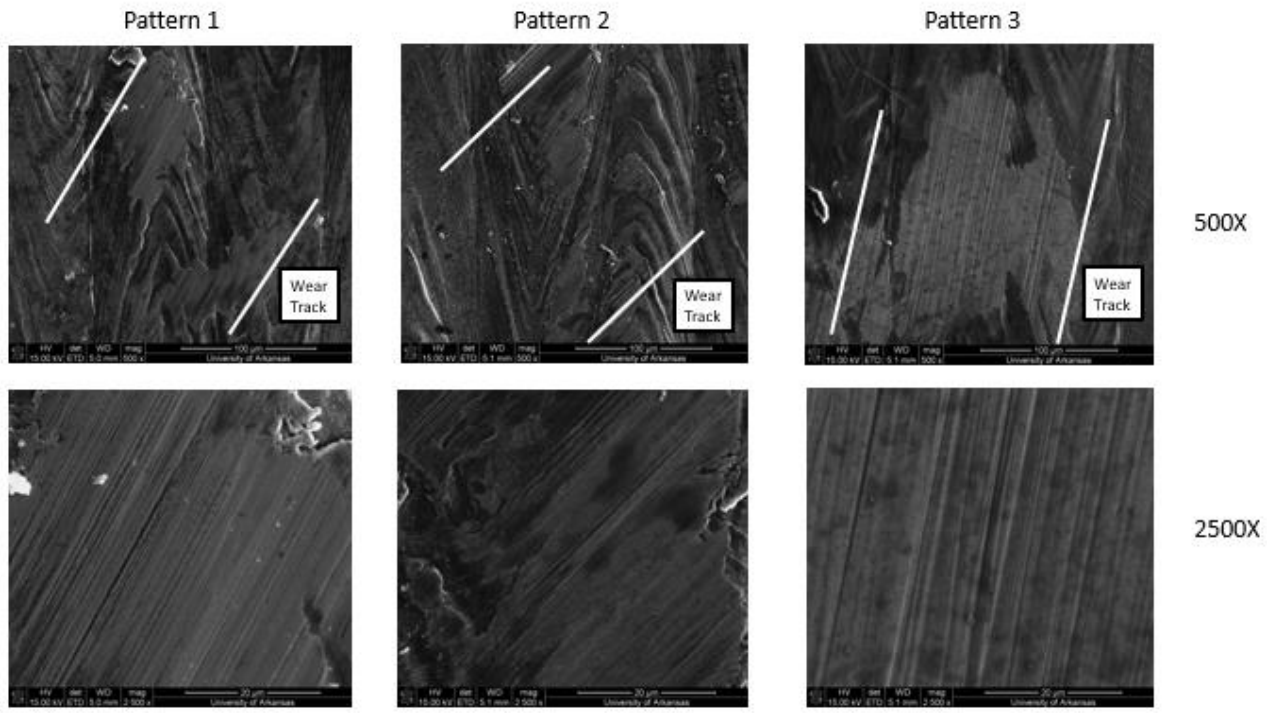


Figure 26. Wear track of all patterns at 500x and 2500x taken at a location where ball travelled at a 45 degree angle to the texture orientation.

Figures 25 and 26 show at 500x and at 2500x wear track patterns when the ball was traveling at different angles with respect to the denticulational micro texture. As seen, even though the ball was traveling at different angles, the wear track approximate width and shape were similar. However, the wear track in the parallel direction was not as continuous compared to its angled counterparts. This occurrence was due to the u-shaped nature of the denticulations and the bumps it created, causing the balls travel to not be continuous.

In addition, energy dispersive x-ray (EDX) spectroscopy scans were taken along the wear track to determine what elements were present from the tribological testing. It was shown that phosphorus was only present along the wear track and not on the remainder of the sample. Examples of this occurrence are shown in Figure 27. This was attributed to the creation of a tribofilm on the surface. This tribofilm was created due to a frictional chemical reaction in which

the COF drove the reaction to create a tribofilm, therefore leaving trace amounts of phosphorus on the surface of the wear track.

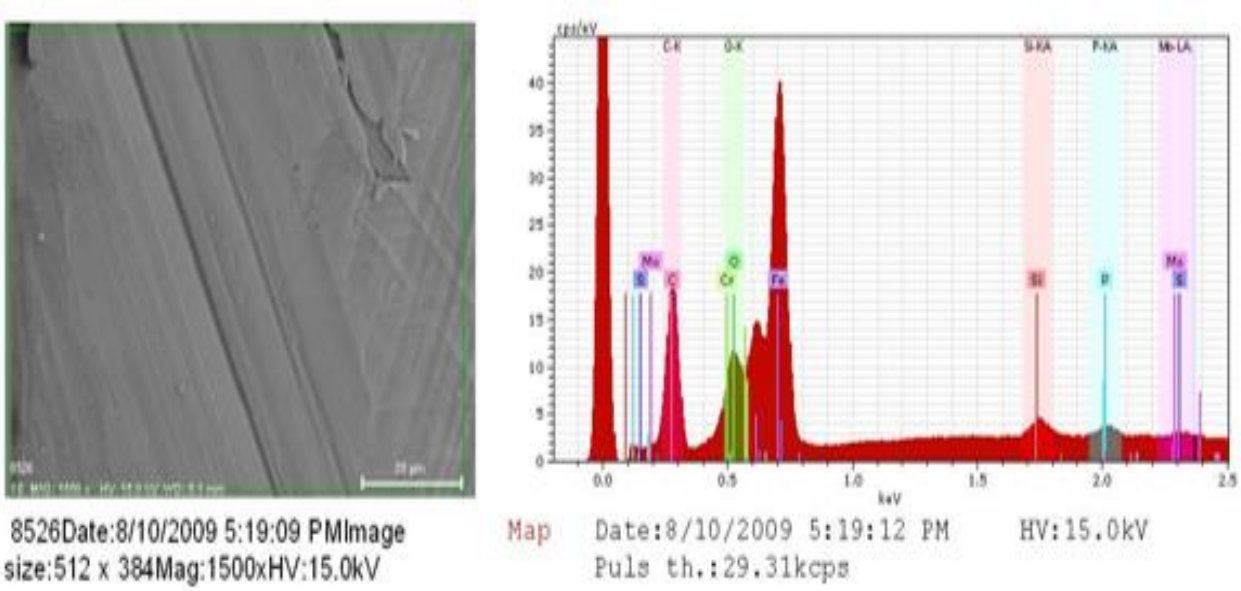


Figure 27. EDX map of the wear track.

The wear tracks were also analyzed using the profilometer to determine the features of the wear tracks at different locations along the circular track. Using these images, it was possible to observe the effects of the wear on all three patterns and how the frictional response changed due to the effects of the different surface features. It was found that $R_q$ tended to be lower when the wear track was analyzed parallel to the micro texture and highest when facing backwards to the parallel direction. It was concluded that even after the surface has been thoroughly worn, the general effects of the micro texture were still prevalent.

### 4.4 Summary

Overall. throughout all experiments, there was a clear sinusoidal trend in the COF behavior at the ball and texture interface. It demonstrated the frictional anisotropy that was

manifested of the ball surface anisotropically interacting through the changing orientation of the micro texture on the 3D printed scales. As a result, it could be shown that the traction was controllable by means of periodic modulation of the texture orientation, allowing for the manipulation of the frictional properties, as observed in the case of snake locomotion.

# Chapter 5

## Conclusion

This research focused on the convergence of biological design (snake skin), manufacturing of the snake skin inspired macro- and micro- hierarchical texture, and their functional properties for frication manipulation. After detailed literature review using a real snake skin, hierarchical patterning and orientation of the scales were studied and analyzed using a non-contact optical surface profilometer. A snake skin-inspired 3D design was created and manufactured using a laser-powder bed fusion (L-PBF) process using 420 stainless steel as powder material. In one step, this process could replicate the macro- and directional micro textures found within the specified hexagonal shaped macro pattern. Through the surface texture characterization, it was also found that the roughness of the steel samples was consistent and comparable to natural snake skin.

To determine if the modeled 3D pattern recreated the anisotropic frictional properties of snakes, tribological tests and analysis were conducted on the surface of the 3D printed parts. All of the printed 3D samples showed clear anisotropic frictional properties as represented by the sinusoidal pattern during frictional testing. In addition, the steel samples demonstrated a clear capability for the micro texture to directly affect the outcome by manipulating the traction on the surface of materials by managing the coefficient of friction by changing the patterning of the micro textures. As a final conclusion, this feasibility research showed successful convergence of bio-inspired design using a 3D printing process for manufacturing of hierarchical surface textures for functional application. In the future, continued optimization of the surface parameters and micro texture could be pursued and studied. As each species of snake has its own unique micro patterning, macro patterning, and overall scale design, further frictional analysis

could be performed, and the outcome determined by the number of features on the overall pattern.

## References


1. Malshe, A. P., Bapat, S., Rajurkar, K. P., and Haitjema, H., 2018, "Bio-Inspired Textures for Functional Applications," CIRP Ann., **67**(2), pp. 627–650.

2. Malshe, A., Rajurkar, K., Samant, A., Hansen, H. N., Bapat, S., and Jiang, W., 2013, "Bio-Inspired Functional Surfaces for Advanced Applications," CIRP Ann. - Manuf. Technol., **62**(2), pp. 607–628.

3. Baum, M. J., Heepe, L., Fadeeva, E., and Gorb, S. N. (2014). Dry friction of microstructured polymer surfaces inspired by snake skin. *Beilstein Journal of Nanotechnology,* **5**(1), 1091-1103.

4. "Color Patterns & Scales Structure." *Color Patterns & Scales Structure :: Florida Museum of Natural History*. [Online]. [Accessed: 9-Oct-2018]. https://www.floridamuseum.ufl.edu/herpetology/fl-snakes/color-pattern/.

5. Micu, A., "Research of Snakes' Straight-Line Movement Could Power the Rescue Bots of the Future" [Online]. [Accessed: 15-Nov-2018]. https://www.zmescience.com/science/snake-movement-straight-line/.

6. Abdel-Aal, H. A., 2013, "On Surface Structure and Friction Regulation in Reptilian Limbless Locomotion," J. Mech. Behav. Biomed. Mater., **22**, pp. 115–135.

7. Lee, M. (2014). Snake skin: Small scales with a large scale impact. (pp. 103-114) Springer International Publishing.

8. Peters, J. A., and Wallach, V., 2018, "Snake," Encycl. Br. [Online]. [Accessed: 21-Jul-2018].

9. Ripamonti, A., Alibardi, L., Falini, G., Fermani, S., and Gazzano, M. (2009). Keratin-lipid structural organization in the corneous layer of snake. *Biopolymers - Peptide Science Section*, **91**(12), pp. 1172-1181.

10. Hu, Y., Ding, J., Yang, J., Fan, Z., Zhang, Z., Zhang, H., and Dai, Z. (2006). Bio-friction properties of snake epidermis scales. *Run Hua Yu Mi Feng/Lubrication Engineering,* (11), pp. 56-59.

11. Abdel-Aal, H. A., El Mansori, M., and Mezghani, S., 2010, "Multi-Scale Investigation of Surface Topography of Ball Python (Python Regius) Shed Skin in Comparison to Human Skin," Tribology Letter, **37**(3), pp. 517–527.

12. Filippov, A. E., and Gorb, S. N., "Modelling of the Frictional Behaviour of the Snake Skin Covered by Anisotropic Surface Nanostructures," Sci. Rep., **6**(August 2015), pp. 1–6.

13. "What Can Snakes Teach Us About Engineering Friction?" *DrexelNow*, [Online]. [Accessed: 16-Feb-2019]. https://drexel.edu/now/archive/2018/May/snake-skin-surface-design/.

14. Gray, B. Y. J., 1946, "The Mechanism of Locomotion in Snakes," **23**(2). pp. 101-120.

15. “Surface Roughness Parameters” [Online]. [Accessed: 8-Feb-2019]. https://www.keyence.com/ss/products/microscope/roughness/line/parameters.jsp.

16. Hu, D. L., Nirody, J., Scott, T., and Shelley, M. J., 2009, “The Mechanics of Slithering Locomotion,” Proc. Natl. Acad. Sci., **106**(25), pp. 10081–10085.

17. *ISO*, www.iso.org/obp/ui/#iso:std:iso:25178:-2:ed-1:v1:en. [Online]. [Accessed: 15-Feb-2019].

18. Blateyron, F., 2013, “The Areal Field Parameters,” *Characterisation of Areal Surface Texture*, R. Leach, ed., Springer Berlin Heidelberg, pp. 15–43.

19. Abdel-Aal, H. A., 2016, “Functional Surfaces for Tribological Applications: Inspiration and Design,” Surf. Topogr. Metrol. Prop., **4**(4), pp. 043001.

20. Abdel-Aal, H. A, and El Mansori, M., 2013, “Tribological Analysis of the Ventral Scale Structure in a Python Regius in Relation to Laser Textured Surfaces,” Surf. Topogr. Metrol. Prop., **1**(1), p. 015001.

21. Abdel-Aal, H. A. (2015) “The Structure of Ventral Scale Textures in Snakes in Comparison to Texturing of Deterministic Tribological Surfaces.” In R. Tyagi, & J. Davim (Eds.), *Processing Techniques and Tribological Behavior of Composite Materials.* IGI Global. Hershey, PA pp. 268–315.

22. Baum J., Heepe, L., Gorb, S. N. (2014). Friction behavior of a microstructured polymer surface inspired by snake skin. *Beilstein Journal of Nanotechnology,* **5**(1), 83-97.

23. Baum, M. J., Kovalev, A. E., Michels, J., and Gorb, S. N. (2014). Anisotropic friction of the ventral scales in the snake lampropeltis getula californiae. *Tribology Letters,* **54**(2), pp. 139-150.

24. Benz, M. J., Kovalev, A. E., and Gorb, S. N. (2012). Anisotropic frictional properties in snakes. Paper presented at the *Bioinspiration, Biomimetics, and Bioreplication 2012, March 12, 2012 - March 15,* Optical Instrumentation Engineers (SPIE).

25. Bhasi, K., Riga, A. T., and Alexander, K. S. (2004). Characterization of snake skin by thermoanalytical techniques. *Journal of Thermal Analysis and Calorimetry,* **75**(1), pp. 269-276.

26. Brannon, Heather. “Which Part of the Skin Protects You From Injury?” *Verywell Health*. [Online]. [Accessed: 16-June-2019]. https://www.verywellhealth.com/anatomy-of-epidermis-1068881.

27. Chang, A. H., and Vela, P. A. (2019). Evaluation of bio-inspired scales on locomotion performance of snake-like robots. *Robotica.* **37**(8), pp.1302-1319.

28. Cuervo, P., Lopez, D. A., Cano, J. P., Sanchez, J. C., Rudas, S., Estupinan, H., and Abdel-Aal, H. (2016). Development of low friction snake-inspired deterministic textured surfaces. *Surface Topography: Metrology and Properties,* **4**(2), pp.024013.

29. DesertUSA.com. “The Royal Python (Ball Python).” *DesertUSA*. [Online]. [Accessed: 20-Mar-2019]. https://www.desertusa.com/reptiles/ball-python.html.

30. Filippov, A. E., Westhoff, G., Kovalev, A., and Gorb, S. N. (2018). Numerical model of the slithering snake locomotion based on the friction anisotropy of the ventral skin. *Tribology Letters,* **66**(3), pp.66-119.

31. Gadelmawla, E. S., Koura, M. M., Maksoud, T. M. A., Elewa, I. M., and Soliman, H. H., 2002, “Roughness Parameters,” J. Mater. Process. Technol., **123**(1), pp. 133–145.

32. Graf, Alex. “Python Regius (Ball Python, Royal Python).” *Animal Diversity Web*. [Online]. [Accessed: 27-Nov-2018]. https://animaldiversity.org/accounts/Python_regius/.

33. Greiner, C., and Schafer, M. (2015). Bio-inspired scale-like surface textures and their tribological properties. *Bioinspiration and Biomimetics,* **10**(4), pp. 044001.

34. Hazel, J., Stone, M., Grace, M., and Tsukruk, V., 1999, “Nanoscale Design of Snake Skin for Reptation Locomotions via Friction Anisotropy,” J. Biomech., **32**(5), pp. 477–484.

35. Irrinki, H., Dexter, M., Barmore, B., Enneti, R., Pasebani, S., Badwe, S., Stitzel, J., Malhotra, R., and Atre, S. V., 2016, “Effects of Powder Attributes and Laser Powder Bed Fusion (L-PBF) Process Conditions on the Densification and Mechanical Properties of 17-4 PH Stainless Steel,” JOM, **68**(3), pp. 860–868.

36. Khan, R., Billah, M. M., Watanabe, M., and Shafie, A. A. (2013). Development of a novel locomotion algorithm for snake robot. Paper presented at the *5th International Conference on Mechatronics, ICOM 2013, July 2, 2013 - July 4,* **53**(1).

37. Kim, J., Varenberg, M. (2019). Contact splitting in dry adhesion and friction: Reducing the influence of roughness. *Beilstein Journal of Nanotechnology,* **10**(1), pp. 1-8.

38. Kovalev, A., Filippov, A., Gorb, S. N. (2016). Correlation analysis of symmetry breaking in the surface nanostructure ordering: Case study of the ventral scale of the snake morelia viridis. *Applied Physics A: Materials Science and Processing,* **122**(3), pp.1-9.

39. Leach, R. K., 2010, “Surface Topography Measurement Instrumentation,” *Fundamental Principles of Engineering Nanometrology*, Elsevier, Oxford; Amsterdam, pp. 115–175.

40. Martinez, A., and Palumbo, S. (2018). Anisotropic shear behavior of soil-structure interfaces: Bio-inspiration from snake skin. Paper presented at the *3rd International Foundation Congress and Equipment Expo 2018: Innovations in Ground Improvement for Soils, Pavements, and Subgrades, IFCEE 2018,* pp. 94-104.

41. Marvi, H., Meyers, G., Russell, G., and Hu, D. L. (2011). Scalybot: A snake-inspired robot with active control of friction. Paper presented at the *ASME 2011 Dynamic Systems and Control Conference and Bath/ASME Symposium on Fluid Power and Motion Control, DSCC 2011, October 31, 2011 - November 2,* pp. 443-450.

42. Mothe, C. G., Mothe, M. G., Riga, A. T., and Alexander, K. S. (2011). Thermal analysis of a model bio-membrane: Human and snake skins. *Journal of Thermal Analysis and Calorimetry,* **106**(3), pp. 637-642.

43. Nath, S. D., Irrinki, H., Gupta, G., Kearns, M., and Atre, S. V., 2019, "Effects of Layer Thickness in Laser-Powder Bed Fusion of 420 Stainless Steel," [Online]. [Accessed: 4-June-2018]. www.researchgate.net/publication/325532825_Laser-Powder_Bed_Fusion_of_420_Stainless_Steel_for_Mold_and_Surgical_Tool_Applications.

44. Nath, S. D., Rajan, A., Yeung, J., and Atre, S. V., 2018, "AM for the OR: Laser-Powder Bed Fusion Delivers Laparoscopic Instruments," 3D Met. Print. Mag. [Online]. [Accessed: 4-June-2018]. https://www.3dmpmag.com/magazine/article/?/2018/2/9/AM_for_the_OR:_Laser-Powder_Bed_Fusion_Delivers_Laparoscopic_Instruments.

45. Nath, S. D., Irrinki, H., Gupta, G., Kearns, M., Gulsoy, O., and Atre, S. V., 2018, "Microstructure-Property Relationships of 420 Stainless Steel Fabricated by Laser-Powder Bed Fusion," Powder Technol, **343**(1), pp.738-746.

46. Palermo, Elizabeth. "What Is Selective Laser Sintering?" *LiveScience*, Purch, 13 Aug. 2013. [Online]. [Accessed: 17-Jan-2019. https://www.livescience.com/38862-selective-laser-sintering.html.

47. Ren, L., Li, B., Song, Z., Liu, Q., Ren, L., and Zhou, X. (2019). 3D printing of bioinspired structural materials with fibers induced by doctor blading process. *International Journal of Precision Engineering and Manufacturing - Green Technology,* **6**(1), pp. 89-99.

48. Serrano, M. M., Chang, A. H., Zhang, G., and Vela, P. A. (2015). Incorporating frictional anisotropy in the design of a robotic snake through the exploitation of scales. Paper presented at the *2015 IEEE International Conference on Robotics and Automation on,* pp. 3734, 2015.

49. "Snake Locomotion" [Online]. [Accessed: 01-Nov-2018]. https://userweb.ucs.louisiana.edu/~brm2286/locomotn.htm.

50. Sun, Y., and Guo, Z. (2019). "Recent advances of bioinspired functional materials with specific wettability: From nature and beyond nature." *Nanoscale Horizons, 4*(1), 52-76.

51. Suresh, S. A., Kerst, C. F., Cutkosky, M. R., and Hawkes, E. W. (2019). Spatially variant microstructured adhesive with one-way friction. *Journal of the Royal Society Interface,* **16**(150).

52. Wang, X., Osborne, M. T., and Alben, S. (2014). Optimizing snake locomotion on an inclined plane. *Physical Review E - Statistical, Nonlinear, and Soft Matter Physics,* **89**(1), pp. 012712.

53. Xiao, X., & Murphy, R. (2018). "A review on snake robot testbeds in granular and restricted maneuverability spaces." *Robotics and Autonomous Systems,* **110**, pp. 160-172.

54. Yang, W., Meyers, M. A., & Ritchie, R. O. (2019). "Structural architectures with toughening mechanisms in nature: A review of the materials science of type-I collagenous materials." *Progress in Materials Science,* **103**, 425-483.

55. Yu, H., Li, J., Chen, Y., Li, J., Liu, L., and Chen, X. (2019). “Analysis of strengthening and toughening mechanisms of bioinspired mineral bridges on hot-pressed alumina-based ceramics through finite element method, **45**(9), pp. 11251-11257.

56. Zheng, L., Zhong, Y., Gao, Y., Li, J., Zhang, Z., Liu, Z., and Ren, L. (2018). Coupling effect of morphology and mechanical properties contributes to the tribological behaviors of snake scales. *Journal of Bionic Engineering,* **15**(3), pp. 481-493.

57. Zhu, N., Zang, H., Liao, B., Liu, D., Tuo, J., Zhou, T., and Wang, Q. (2018). “The effect of different scales on the crawling rate of bionic snake robot.” Paper presented at the *1st WRC Symposium on Advanced Robotics and Automation, WRC SARA 2018, August 16,* pp. 22-27.

58. Zug, George R. “Locomotion.” *Encyclopædia Britannica*, Encyclopædia Britannica, Inc. [Online]. [Accessed: 31-Aug-2017]. https://www.britannica.com/topic/locomotion.

# Appendix

## Appendix A: Description of Research for Popular Publication

In the field of mechanical engineering, the efficiency of designs is crucial in relation to the operation of the whole. However, to improve on an entire system, you need to improve the individual parts. By improving each part, no matter how small, one can increase the overall usefulness of the system. As the demands of the consumers continue to grow due to the rise in population, the performance of many different products must also continue to rise alongside the increase to satisfy these needs. Catherine Tiner, a Master's student in the Microelectronics-Photonics Graduate Program at the University of Arkansas, has devised a potential way to counteract these problems while satisfying demands.

With the newly entered Industry 4.0 age developing quickly, a reliance is forming on the reliability of advancements in machining and other industries. As envisioned by both Tiner and Dr. Ajay Malshe, it is possible to create new sustainable products based on the advancements seen in the nature surrounding us.

As the earth is continuously changing all around us, the species that live on the planet must adapt and change to be able to continue to survive. It is not the strongest or even the smartest animal that survives this evolutionary change, it is the one most willing to adapt. It was found that snakes are the best example of evolution and adaptation. While snakes have no legs, arms, other appendages, they are still capable of traversing all realms of terrain quickly and efficiently. By studying the locomotional abilities of snakes, Tiner and Malshe concluded that the unique ability of a snake to effectively move forward could be redesigned and recreated for our own purposes. But how could snakes be used in industry settings? The two seem entirely

different in theory. However, they are actually quite similar in capabilities. Snake skin possesses anisotropic frictional properties. This means that snakes can move effortlessly forward. However, a snake has a rough time moving backward. This is why you rarely, if ever, see a snake moving backward. They are always moving forward as it is much easier for them to move in that direction!

By recreating this functionality, advancements can be explored for one directional movement applications. While the idea of snake inspired applications may seem scary to those afraid of reptiles, these reptiles themselves may be just what we need to continue our advancements into a new age.

## Appendix B: Executive Summary of Newly Created Intellectual Property

The following list indicates newly created intellectual items.

1. Design and creation of 3D printed snake skin using an L-PBF process.
2. Construction of snake skin inspired micro texture using 3D modeling tools.

## Appendix C: Possible Patent and Commercialization Aspects of Intellectual Property

### C.1 Patentability of Intellectual Property

Each of the previous items were considered for their potential patentability. However, it was decided that none of the items mentioned above could be patented. Detailed descriptions follow.

1. While the creation of a snake skin itself is new, the technology used to create this micro texture has been utilized in many ways before. Since the overall process itself is not unique, the idea is not patentable.
2. The micro texture that was inspired from snake skin, while distinctive, is not a consistent pattern due to each snake possessing a different general pattern of hierarchical orientation. Due to the potential inconsistencies, this texture pattern is not patentable.

### C.2 Commercialization Aspects

Each of the previous items were considered for commercialization potential. However, it was decided that none of the items mentioned above have commercial need or appeal. A detailed description follows.

1. The snake skin outline pattern is a viable tool for frictional research. However, the pattern itself is not unique and has been used many times in different industries. While the skin would be of interest to those in the biological or engineering fields, the snake skin itself is not of interest to others.
2. The micro texture similarly doesn't exhibit a commercial appeal. While those in the friction field might properly utilize the anisotropic frictional properties found on the skin, the texture would only be of interest to a niche group.

## C.3 Possible Future Disclosure of Intellectual Property

Both the macro and micro texture patterns found on snake skin have been prepared and presented to the North American Manufacturing Research Conference in 2019. This research paper was published by Tiner as the lead author.

## Appendix D: Broader Impact of Research

### D.1 Applicability of Research Methods to Other Problems

Recently, both engineers and research scientists have been inspired by the nature that surrounds them. The impacts of bio-inspired engineering have become more and more relevant over time. Of recent interest, the designs found in nature have been adapted for industrial use. This research was conducted using stainless steel in hopes that this micro textured pattern could be used for unidirectional applications such as rails, gears, and related gantry systems.

### D.2 Impact of Research Results on U.S. and Global Society

Textures in nature are the source of different superior functionalities and have allowed for the survival of an abundance of different species. As industry 4.0 continues to develop, a need for more efficient methods of development has been discovered. Currently, problems in system manufacturing and engineering processes include throughput and production. By taking inspiration from nature, these processes can be expanded upon to benefit the system as a whole. As the micro textures developed in this research is beneficial to specific applications and operations moving in a singular direction, this design has the potential to broaden the learning conducted by bio-inspired engineering while inspiring others to continue learning from what nature has to offer.

### D.3 Impact of Research Results on the Environment

As this research focuses on taking inspiration from nature, the effects of this research on the environment have been studied. By utilizing this research in manufacturing and industrial settings, the implementation of the micro textures allows for increased reliability and efficiency. This in turn would lower the negative impact on the environment.

## Appendix E: Microsoft Project for M.S. MicroEP Degree Plan

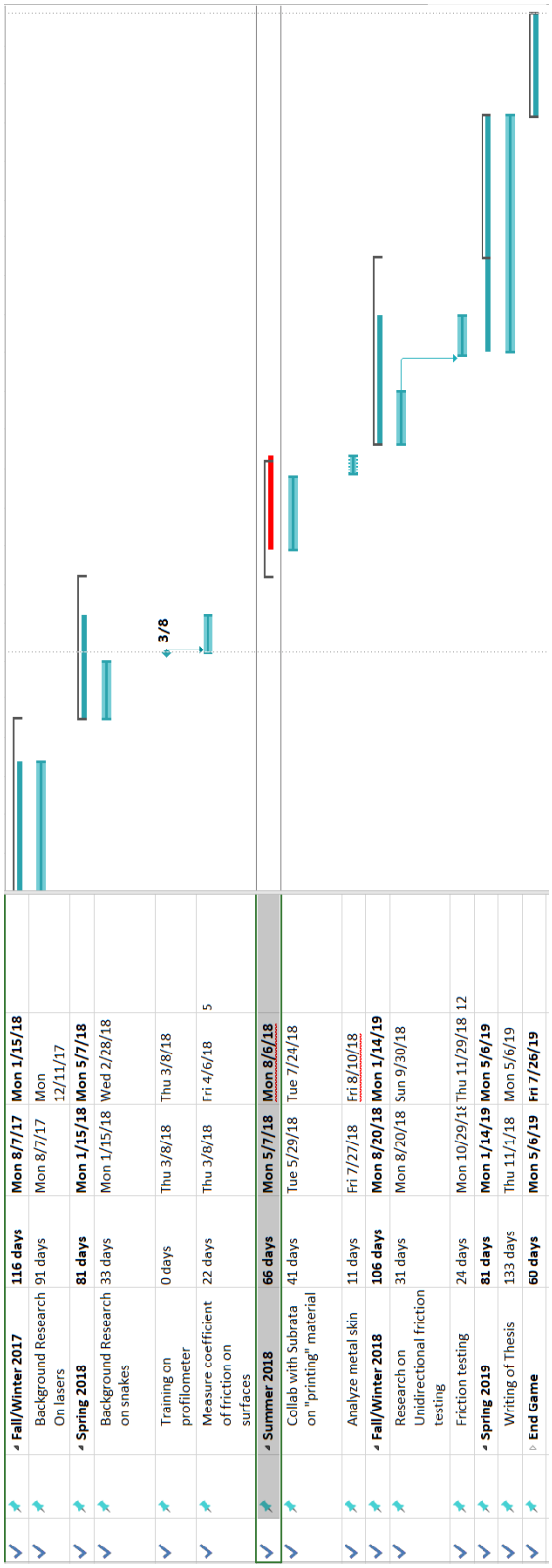


| | Task Name | Duration | Start | Finish | Predecessors |
|---|---|---|---|---|---|
| | Fall/Winter 2017 | 116 days | Mon 8/7/17 | Mon 1/15/18 | |
| | Background Research On lasers | 91 days | Mon 8/7/17 | Mon 12/11/17 | |
| | Spring 2018 | 81 days | Mon 1/15/18 | Mon 5/7/18 | |
| | Background Research on snakes | 33 days | Mon 1/15/18 | Wed 2/28/18 | |
| | Training on profilometer | 0 days | Thu 3/8/18 | Thu 3/8/18 | |
| | Measure coefficient of friction on surfaces | 22 days | Thu 3/8/18 | Fri 4/6/18 | 5 |
| | Summer 2018 | 66 days | Mon 5/7/18 | Mon 8/6/18 | |
| | Collab with Subrata on "printing" material | 41 days | Tue 5/29/18 | Tue 7/24/18 | |
| | Analyze metal skin | 11 days | Fri 7/27/18 | Fri 8/10/18 | |
| | Fall/Winter 2018 | 106 days | Mon 8/20/18 | Mon 1/14/19 | |
| | Research on Unidirectional friction testing | 31 days | Mon 8/20/18 | Sun 9/30/18 | |
| | Friction testing | 24 days | Mon 10/29/18 | Thu 11/29/18 | 12 |
| | Spring 2019 | 81 days | Mon 1/14/19 | Mon 5/6/19 | |
| | Writing of Thesis | 133 days | Thu 11/1/18 | Mon 5/6/19 | |
| | End Game | 60 days | Mon 5/6/19 | Fri 7/26/19 | |

## Appendix F: Identification of All Software Used in Research and Thesis Generation

Computer #1

Model: Dell Inspiron 15 7000 Series

Serial Number: JOV2K22

Location: Home

Owner: Catherine Tiner

Software #1

Name: Microsoft Office, 365

Purchased By: Catherine Tiner

License: YR229-NB77P-JFKKK-JV8VC-P9XQR

Software #2

Name: SolidWorks

Purchased By: University of Arkansas Student Use

License CAD: 9020 0091 0565 4666 6JR3 7SHD

License CAM: 9020 0091 0575 3524 CYD8 5VJ8

## Appendix G: All Publications Published, Submitted, and Planned

Publications Submitted

1. Tiner, C., Bapat, S., Nath, S. D., Atre, S. V., and Malshe, A. (2019). Exploring Convergence of Snake-Skin-Inspired Texture Designs and Additive Manufacturing for Mechanical Traction. Procedia Manufacturing, 34, 640-646. (NAMRC 47 publication).

## Appendix H: Publishing Agreements/Permissions

Elsevier grants permission for authors to use their own articles in full or in part in a thesis or dissertation for non-commercial purposes.
www.elsevier.com/about/policies/copyright/permissions.